

Statistical models for estimating the fatigue life, the stress–life relation, and the P–S–N curves of metallic materials in Very High Cycle Fatigue: A review

Andrea Tridello¹  | Carlo Boursier Niutta¹  | Massimo Rossetto¹  |
Filippo Berto²  | Davide S. Paolino¹ 

¹Department of Mechanical and Aerospace Engineering, Politecnico di Torino, Turin

²Department of Mechanical and Industrial Engineering, Norwegian University of Science and Technology (NTNU), Trondheim, Norway

Correspondence

Andrea Tridello, Department of Mechanical and Aerospace Engineering, Politecnico di Torino, C.so Duca degli Abruzzi 24, 10129 Turin, Italy.
Email: andrea.tridello@polito.it

Funding information

European Union's Horizon 2020, Grant/Award Number: 101006844

Abstract

The research on the Very High Cycle Fatigue (VHCF) response of materials is fundamental to guarantee a safe design of structural components. Researchers develop models for the fatigue life in VHCF, aiming at assessing the stress–life relation and, accordingly, the probabilistic S–N (P–S–N) curves. In the paper, the models for the stress–life relation in VHCF are comprehensively reviewed. The models are classified according to the approach followed for defining the stress–life dependency, that is, power law, probabilistic, fracture mechanics, or Paris law-based approach. The number of failure modes that can be modeled, the statistical distribution for the fatigue life, and the characteristics of the estimated P–S–N curves are also reviewed by analyzing the fitting capability of experimental datasets for each model. This review is supposed to highlight the strengths and weaknesses of the currently available models and guide the future research.

KEYWORDS

duplex S–N curves, fatigue limit, FGA, statistical model, step-wise curves, ultrasonic fatigue tests, very high cycle fatigue (VHCF)

1 | INTRODUCTION

In the last years, the number of research on the Very High Cycle Fatigue (VHCF) response of materials has significantly increased.^{1,2} The VHCF life range corresponds to the fatigue life region beyond 10^7 cycles with a fatigue strength below the traditional fatigue limit in case of high-strength steels^{3–5} or below the knee point for aluminum alloys. Indeed, for the design of components, like car engines and turbine palettes,¹ subjected to fatigue loads for a long time or to high-frequency loads,² the conventional design methodologies based on the assumption

of a fatigue limit above $2 \cdot 10^6$ cycles or 10^7 cycles are not sufficient to guarantee their structural integrity. Accordingly, a large number of results and research have been carried out through the years to assess the mechanisms of crack initiation in the VHCF region and to model the fatigue life behavior through the analysis of the experimental results.

The research activity on the VHCF response of materials focuses on three main research fields. The first one concerns the development of testing equipment capable of reliably assessing the VHCF response of materials in a reasonable testing time,^{1,6,7} also at elevated

This is an open access article under the terms of the Creative Commons Attribution License, which permits use, distribution and reproduction in any medium, provided the original work is properly cited.

© 2021 The Authors. *Fatigue & Fracture of Engineering Materials & Structures* published by John Wiley & Sons Ltd.

temperatures⁸ and to test different materials or joints (e.g., UFTMs for test on adhesives,^{9,10} on welded joints,^{11,12} and on composite materials¹³) under different loading conditions (torsional fatigue tests,^{14–16} biaxial fatigue tests,^{17,18} and under variable loading¹⁹). The second main research field focuses on the assessment of the mechanisms of crack initiation in VHCF. Indeed, it is widely accepted in the literature that the crack in VHCF mainly originates from a defect (initial defect) present within the material volume. The peculiarity of the VHCF failures is that the crack can initiate and propagate even if the stress intensity factor (SIF) associated with the initial defect is below the threshold for crack propagation. The initiation of the fatigue crack is generally accompanied by the formation of a characteristic area close to the initial defect, which is called, depending on the measuring technique, Optically Dark Area (ODA²⁰), Fine Granular Area (FGA^{21,22}), and Granular-Bright Facet (GBF²³). Research efforts are focused on understanding the mechanisms of crack initiation around the initial defect with the FGA formation, which is fundamental for the assessment of the VHCF response. For a comprehensive review on the formation of this characteristic region, the reader is referred to the review paper.²⁴ The third main macroarea of research concerns the development of models for the fatigue life in VHCF. Conventional low-cycle fatigue (LCF) and high-cycle fatigue (HCF) life models cannot, in general, be used for modeling the VHCF response, since the failure origin is different (surface nucleation in LCF–HCF and internal nucleation in VHCF). The formation of the fatigue cracks from defects with the FGA formation should be also considered when modeling the fatigue life. Moreover, the probabilistic S–N (P–S–N) curves should be modified to take into account the occurrence of the two failure modes and a second decreasing trend below the conventional fatigue limit. In the literature, many different models have been proposed throughout the years based on different approaches. A proper modeling of the fatigue life, to assess the stress–life relation and, accordingly, the P–S–N curve, is of fundamental importance for the design of components against VHCF failures.

In the paper, the models for the fatigue life in VHCF are reviewed. The main objective is to analyze and classify the models that define a relation between the fatigue life and the applied stress amplitude in order to estimate the P–S–N curves. Other reviews on this subject have been published in the literature^{25–27}: in particular, Hong and Sun²⁶ highlight the importance of understanding the mechanisms of crack initiation from defects to model the stress–life relationship and proposed the well-known “Numerous Cyclic Pressure” model to explain the formation of the FGA for failures in the VHCF region.

In the first part of the paper, the models for the fatigue limit in VHCF are described and analyzed. In the second part, the models for the fatigue life are critically reviewed, and the approach followed to define the stress–life relation or the statistical distribution of the fatigue life is analyzed. This comprehensive review is supposed to show the strengths and weaknesses of the models currently available in the literature and to guide the future research by highlighting the already addressed research issues and those that should be investigated in the future.

2 | FATIGUE LIMIT IN VHCF

In this section, the models for the VHCF fatigue limit, that is, the threshold for crack propagation in the VHCF region, are reviewed. In order to model the crack initiation with a SIF smaller than the SIF threshold, the influence of the FGA is taken into account. In Section 2.1, the models for the fatigue limit available in the literature are described, analyzing the approaches followed for assessing their formulation.

As highlighted in Section 1, the characteristic area surrounding the initial defect and responsible for the crack initiation has been called in different ways in the literature. For the sake of clarity and uniformity, this region will be called in the following FGA, even if called in a different way in the original paper. Due to the importance of the analysis of the fracture surfaces when the experimental data are analyzed, Figure 1 shows a picture of a fracture surface with a fish-eye morphology, typical of VHCF failures, that we obtained by testing an high-strength steel. The main features, that is, the initial defect, the FGA, and the fish-eye boundary, are highlighted in the figure.

It must be noted that the presence of a fatigue limit in VHCF is still debated in the literature. However, according to the well-known Murakami model, a fatigue limit can be estimated in the presence of defects or of the weakening mechanisms inducing the formation of the FGA, and it corresponds to the stress amplitude at which a crack cannot propagate from a defect. Other authors in the literature assumed the existence of a fatigue limit^{28,29} in presence of defects and, therefore, in the VHCF region. Moreover, according to Mughrabi (in particular to the multistage fatigue life diagrams⁴), the presence of a lower fatigue limit in the VHCF regime can be assumed for Type 2 material (“*Finally, there are reasons to believe that, at sufficiently low-stress levels, there will be a true ultimate fatigue limit (range II)*”). Therefore, according to the literature, we can assume the existence of a fatigue limit in the VHCF region, even if this assumption has to be proven in future research. This section focuses, therefore,

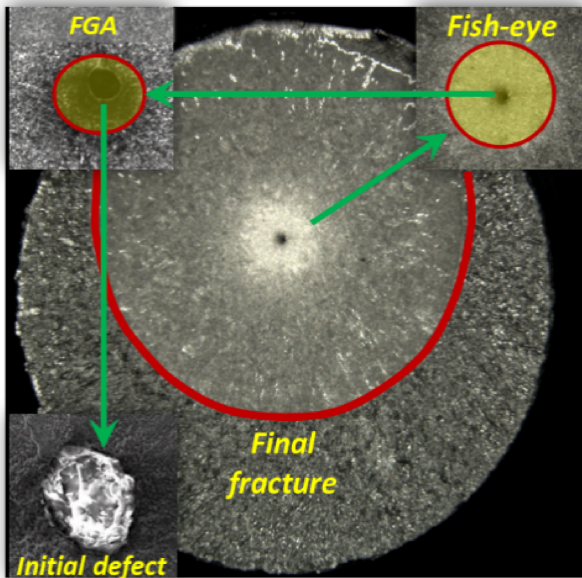


FIGURE 1 Fracture surface typical of failures in the VHCF region with the main features, the initial defect, the FGA, and fish-eye borders highlighted [Colour figure can be viewed at wileyonlinelibrary.com]

on the models that have the objective to propose a formulation for the fatigue limit, that is, a formula that permits to compute the fatigue strength at which the crack does not propagate from defects, since the stress and the weakening mechanisms are not strong enough to originate a fatigue crack.

For what concerns the nomenclature, the area of the initial defect in a direction perpendicular to maximum applied stress (or its equivalent size³⁰) is called $a_{d,0}$ throughout the paper. The number of cycles to failure, the stress amplitude, the SIF threshold, and the fatigue limit are called N_f , s_a , K_{th} , and s_l respectively.

2.1 | Models for the fatigue limit in VHCF

In Murakami,³⁰ an expression for the computation of the fatigue limit in the presence of defects is proposed. The fatigue limit is defined as “the threshold stress for crack propagation and not the critical stress for crack initiation” and is obtained by equating the SIF associated to a defect to the SIF threshold of the material. The fatigue limit depends on the material Vickers hardness, HV , and is inversely proportional to $(\sqrt{a_{d,0}})^{1/6}$ (Murakami³⁰). However, for failures in the VHCF region, the crack originates

from a defect characterized by a SIF smaller than the SIF threshold and starts propagating as a long crack³¹ from the FGA borders. The crack growth within the FGA is possible, according to Murakami,³⁰ due to weakening mechanisms induced by the hydrogen trapped near the initial defect (“hydrogen assisted crack model”). Therefore, differently from failures from defects in HCF, the initial defect area corresponds to the area including the initial defect and the FGA, $\sqrt{(a_{d,0} + a_{FGA})}$, being a_{FGA} the size of the ODA surrounding the initial defect with size $a_{d,0}$, according to Equation 1:

$$s_l = \frac{C \cdot (HV + 120)}{(\sqrt{(a_{d,0} + a_{FGA})})^{1/6}} \cdot \left[\frac{1 - R}{2} \right]^\alpha, \quad (1)$$

where C is a constant coefficient depending on the defect location (e.g., $C = 1.56$ for internal defects) and R is the stress ratio, defined as the ratio between the minimum applied stress, s_{min} , and the maximum applied stress, s_{max} , in a load cycle, and α is a constant coefficient depending on HV ($\alpha = 0.226 + HV \cdot 10^{-4}$). Equation 1 enables to easily compute the fatigue limit in the VHCF regime and to prevent failures characterized by crack initiation with ODA formation.

The validity of Equation 1 modified for VHCF failures was proved in Murakami and Yamashita,³² as shown in Figure 1, which plots the ratio between the applied stress amplitude and the fatigue limit with respect to N_f . In the figure, $\sigma = s_a$ and $\sigma_w = s_l$. The experimental data have been collected by testing, through tension–compression fatigue tests at stress ratio $R = -1$, the heat-treated hard steel Cr-Mo SCM435 steel. In Figure 2, QT refers to the “quenched and tempered” condition, whereas VQ refers to the “quenched in vacuum” conditions. According to Figure 2, almost all fatigue failures occur for σ/σ_w larger than 1, whereas runout specimens are characterized by a ratio σ/σ_w smaller than 1.

A similar approach is followed in Chapetti et al.^{33,34} The threshold for crack propagation is equaled to the SIF associated to an inclusion with radius R_i^{max} (i.e., the radius of the largest inclusion within the material) in order to obtain an expression for the internal fatigue limit, s^{int} at stress ratio $R = -1$ (according to Chapetti et al., “the stress level below which fracture produced by cracks initiated from an internal inclusion is not found after 10^{10} cycles”). It is worth noting that the internal fatigue limit corresponds to the stress amplitude below which a crack does not form even if its formation is assisted by the weakening mechanisms that originate the FGA around defects with a SIF smaller than the SIF threshold.

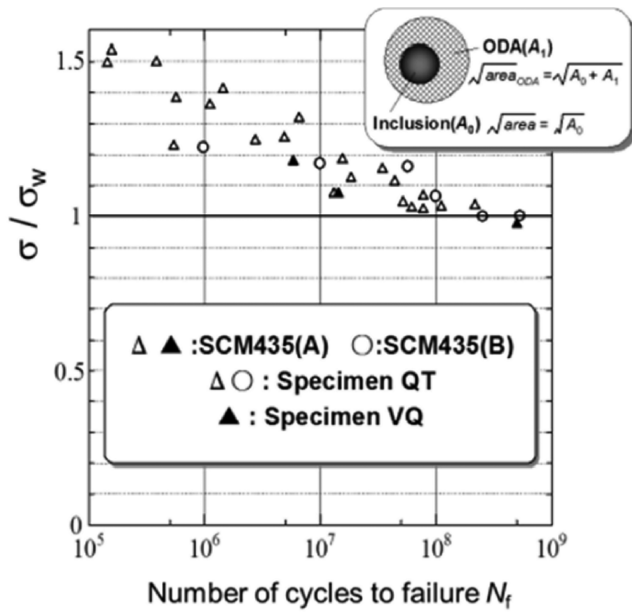


FIGURE 2 Experimental validation of the model for the fatigue limit³²: ratio between the fatigue limit in Equation 1 and the applied stress amplitude with respect to N_f (reprinted with permission from Elsevier)

$$s^{int} = \frac{3.55 \cdot (HV + 120)}{2 \cdot (3 \cdot R_i^{max})^{1/6}} = 256 \cdot \frac{\Delta K_{th}}{\sqrt{R_i^{max}}}, \quad (2)$$

with

$$\begin{cases} \Delta K_{th} = 4 \cdot 10^{-3} (HV + 120) \cdot (3 \cdot R_i^{max})^{1/3} & \text{if } \Delta K_{th} < 10 \text{ MPa}\sqrt{\text{m}}, \\ \Delta K_{th} = 10 \text{ MPa}\sqrt{\text{m}} & \text{if } \Delta K_{th} \geq 10 \text{ MPa}\sqrt{\text{m}}. \end{cases} \quad (3)$$

For the computation of the internal fatigue limit, a crack three times larger than the largest inclusion has been considered (i.e., $3 \cdot R_i^{max}$), since the weakening mechanism inducing the ODA formation, that is, “the hydrogen embrittlement process assisted by fatigue,” takes place within a region with a maximum extension equal to three times the inclusion radius computed from the center of the inclusion. Accordingly, the zone influenced by the inclusion is conservatively assumed as the size of a sphere with radius three times larger than the radius of the initial inclusion. The model has been validated on experimental datasets on high-strength steels available in the literature (the results are reported in a tabular form in the original paper) and proved to be in most cases conservative, with Chapetti et al. pointing out however the need for further validations to assess the limits of the proposed equations.

The macromechanical models in Ref.^{28,35,36} permit assessing the fatigue limit by analyzing the mechanisms of crack initiation in the vicinity of the initial defect. In particular, in Liu et al.,^{28,35} the fatigue limit is estimated by adding a SIF, correlated to the hydrogen concentrated near the initial defect, to the SIF computed by considering the initial defect size. Accordingly, the total SIF for the defect, K_T , is given by the sum of the maximum SIF associated with the initial defect, $K_{I_{max}}$, and the SIF that models the detrimental presence of hydrogen near the defect, K_H . K_H is obtained from literature models accounting for the amount of hydrogen concentrated in the material and is dependent on the coefficient C_0 , i , the initial mass fraction of hydrogen in the cyclic plastic zone around the defect. Liu et al. moreover estimated the SIF threshold at the periphery of the GBF, $(K_{GBF})_{th}$, by analyzing the fracture surfaces of six steels (four spring steels and two bearing steels) subjected to fully reversed ultrasonic fatigue tests up to 10^9 cycles.³⁵ The expression for $(K_{GBF})_{th}$ was found to be equal to that obtained by Murakami for the SIF threshold (eq. 5.4 in Murakami³⁰) but with different coefficients. Through an analysis of the SIF close to the initial defect, the authors conclude that the crack propagation is possible only if the condition $K_T = K_{I_{max}} + K_H = (K_{GBF})_{th}$ is fulfilled. With some passages, the authors obtained the following expression for the fatigue limit $s_{l,LIU}$:

$$s_l = C \cdot \frac{(HV + 120)^{0.9375}}{(\sqrt{a_{d,0}})^{0.1875}}, \quad (4)$$

being C a constant coefficient that can be estimated analytically and experimentally. The authors pointed out that C has to be estimated from the experimental data, since it can be hardly estimated analytically due to the large uncertainty in the coefficients involved in the analytical expression. For the investigated high-strength steels (18 high-strength steels subjected to fully reversed ultrasonic tension–compression fatigue tests were considered), C was found to be equal to 2.7. For inclusion sizes larger than $6 \mu\text{m}$, the model is in good agreement with the experimental data, as shown in Figure 3, which plots the fatigue limit ($\sigma_w = s_l$) normalized by the quantity $(HV + 120)^{0.9375}$ with respect to the initial defect size ($\sqrt{area_{in}} = \sqrt{a_{d,0}}$). All the data are within an error band $\pm 15\%$.

In Paolino et al.,³⁶ the models available in the literature are generalized, and the intrinsic randomness associated with the VHCF phenomena is considered in a statistical framework. Starting from the “hydrogen assisted crack growth” theory proposed by Murakami,³⁰ the SIFs involved in the crack initiation phase in VHCF

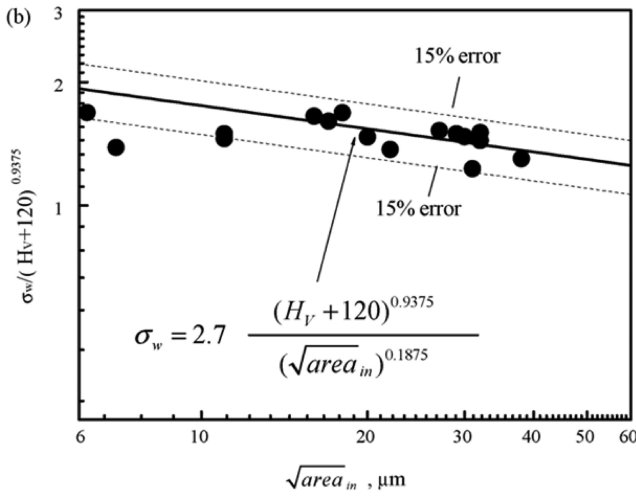


FIGURE 3 Validation of the fatigue model in Liu et al.²⁸: fatigue limit ($\sigma_w = s_l$) normalized by the quantity $(HV + 120)^{0.9375}$ with respect to the initial defect size ($\sqrt{area_{in}} = \sqrt{a_{d,0}}$) (reprinted with permission from Elsevier)

failures have been defined and generalized. In particular, the SIF threshold range, Δk_{th} , has been expressed as

$$\Delta k_{th} = 10^{-3} \cdot c_{th} \cdot (HV + 120) \cdot \sqrt{a_{d,0}}^{\alpha_{th,t}}, \quad (5)$$

being c_{th} and α_{th} constant coefficients. The hydrogen assistance has been modeled with an additional SIF with the following formulation:

$$k_H = 10^{-3} \cdot c_H \cdot s_a \cdot \sqrt{a_{d,0}}^{0.5-\alpha_H} \cdot \sqrt{a_d}^{\alpha_H}, \quad (6)$$

being $\sqrt{a_d}$ the square root of the defect area (i.e., the area of the forming FGA) and c_H and α_H constant coefficients. The total SIF at the crack tip, k_T , is given by the sum of the SIF associated with the initial defect, k_d , and k_H (i.e., $k_T = k_d + k_H$). The crack growth could occur only if $k_T > k_{th}$. According to the Paolino et al., four different scenarios are possible:

1. crack initiation and propagation directly from the initial defect;
2. crack initiation from the defect and following propagation with fish-eye morphology and FGA (in this case $\sqrt{a_d} = \sqrt{a_{FGA}}$);
3. crack initiation with FGA formation but crack arrest and infinite life;
4. crack does not initiate even with the hydrogen assistance.

From this analysis, the following expression for the fatigue limit was obtained:

$$s_l = \frac{c_{sl} \cdot c_{th} \cdot (HV + 120)}{(\sqrt{a_{d,0}})^{0.5-\alpha_{th,t}}}, \quad (7)$$

being c_{sl} a constant coefficient that must be estimated from the experimental data and that models the hydrogen assistance (i.e., c_{th} and α_{th} are obtained by analyzing the SIF threshold in Equation 5). The authors moreover showed the procedure for the estimation of the c_{sl} coefficient through the application of the maximum likelihood principle, with the likelihood function expressing the probability of having a failure or a runout for the experimental data. Starting from the statistical distribution of Δk_{th} , it is shown that the logarithm of the fatigue limit is a random variable (rv), $X_l | \sqrt{a_{d,0}}$, that follows a Normal distribution with mean $\mu_{X_l}(\sqrt{a_{d,0}})$ depending on $\sqrt{a_{d,0}}$ and constant standard deviation σ_{X_l} . In Paolino et al.,³⁶ the uppercase has been used for the rv, whereas the lowercase has been used for the realization of the rv (i.e., for deterministic values). The cumulative distribution function (cdf) of $X_l | \sqrt{a_{d,0}}$, $F_{X_l | \sqrt{a_{d,0}}}(x_l; \sqrt{a_{d,0}})$, is given by

$$F_{X_l | \sqrt{a_{d,0}}}(x_l; \sqrt{a_{d,0}}) = \Phi\left(\frac{x_l - \mu_{X_l}(\sqrt{a_{d,0}})}{\sigma_{X_l}}\right)$$

$$\text{with} \begin{cases} \mu_{X_l}(\sqrt{a_{d,0}}) = \frac{c_{sl} \cdot c_{th} \cdot (HV + 120)}{(\sqrt{a_{d,0}})^{0.5-\alpha_{th}}} \\ \sigma_{X_l} = \text{const} \end{cases} \quad (8)$$

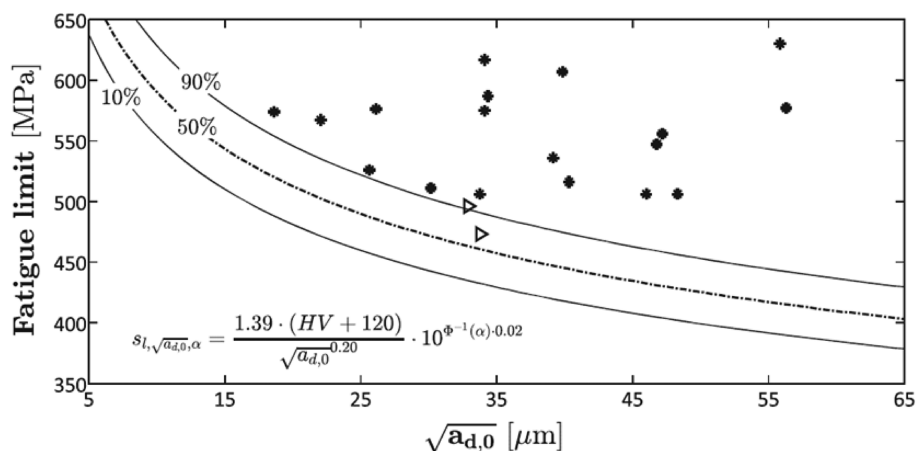
The model has been validated on an experimental dataset obtained by the authors through ultrasonic fully reversed tension-compression fatigue tests on H13 steel specimens. Figure 4 plots the estimated median and 10th and 90th quantiles of the fatigue limit with respect to $\sqrt{a_{d,0}}$ and proves the effectiveness of the proposed model, since all the experimental failures are above the estimated quantiles of the fatigue limit.

According to Equation 8 and Figure 4, as well as for the other models described in this section,^{28,30,32,34,36} the fatigue limit is a function of the defect size. This dependency is eliminated by exploiting the properties of the marginal cdfs and by considering the statistical distribution of the defect size. The cdf of the fatigue limit no more conditioned to the defect size (marginal fatigue limit, $F_{X_l}(x_l)$) is given by

$$F_{X_l}(x_l) = \int_0^{\infty} F_{X_l | \sqrt{a_{d,0}}}(x_l; \sqrt{a_{d,0}}) f_{\sqrt{A_{d,0}}}(\sqrt{a_{d,0}}) d\sqrt{a_{d,0}}, \quad (9)$$

According to the literature,³⁰ $\sqrt{A_{d,0}}$ was assumed to follow a largest extreme value distribution (LEVD). The

FIGURE 4 Validation of the fatigue model in Paolino et al.³⁶: fatigue limit with respect to $\sqrt{a_{d,0}}$ (reprinted with permission from Wiley)



model in Equation 9 was successfully validated, with all the experimental failures above the 90th quantile of the fatigue limit.

A further generalization of the fatigue limit model defined by the research group of the Politecnico di Torino has been proposed in Paolino et al.³⁷ In particular, a reduction SIF $k_{th,r}$ that models the weakening mechanisms for crack initiation from the initial defect is introduced. Accordingly, a local SIF threshold, $k_{th,l}$, associated to the initial defect, has been defined as the difference between the SIF threshold (Equation 9) and the reduction SIF (i.e., $k_{th,l} = k_{th} - k_{th,r}$). In these cases, the unknown parameters have been estimated by minimizing the difference between the number of cycles consumed within the FGA and the number of cycles estimated with the proposed model, by assuming that the crack growth within the FGA can be described with the Paris law (i.e., $da/dN = c_I \cdot (k_d - k_{th,l})^{m_I}$, being c_I and m_I unknown coefficients and k_d the SIF associated with the defect). The model is found to be in agreement with the experimental data, with the experimental failures conservatively above the estimated 90% fatigue limit. The dependency between the fatigue limit and the risk volume (according to Murakami,³⁰ the volume of material subjected to a stress amplitude larger than the 90% of the maximum stress) and the influence of the stress ratio have been also investigated by the research group of the Politecnico di Torino in Paolino et al.^{38–40}

According to the above analysis, the defect and the FGA size affect the crack initiation in VHCF and the fatigue limit. For the Murakami model (Equation 1), the VHCF limit can be estimated only if the FGA size is known, whereas for the other three models, the initial defect size must be considered. The estimation of the defect size is easier than the estimation of the FGA size, which is not known a priori before experimental tests. On the contrary, the defect size can be estimated through different techniques (e.g., inclusion sampling, CT scan).

In order to estimate the FGA size without performing experimental tests, in Murakami and Yamashita,³² a procedure for the estimation of the FGA size from the initial defect size is proposed and based on the “*Master curve of ODA*.” It must be also noted that, even if the formulations in Ref.^{28,35,36} (Equations 4, 8, and 9) depend on the defect size, a preliminary experimental phase is necessary to estimate the constant material coefficients, with procedures requiring the assessment of the FGA size. However, once the coefficients have been estimated, the formulations for the fatigue limit in Ref.^{28,35,36} (Equations 4, 8, and 9) can be easily used by considering the defect size. On the other hand, the model in Chapetti et al.³⁴ can be applied without the need of assessing the FGA size. However, this model (Equation 2) is based on the assumption that the region affected by the hydrogen is a circular region with a radius three times the inclusion radius. This assumption was shown to be valid by Chapetti et al., but it should be also validated on other metallic materials or if different weakening mechanisms are responsible for the crack growth within the FGA.

In general, all the analyzed fatigue limit formulations point out the need of reliably assessing or estimating the defect and the FGA size. Moreover, apart from the formulation in Paolino et al.³⁶ (Equations 8 and 9), the statistical scatter is not taken into account, and the quantiles of the fatigue limit are not defined, despite their importance when components are to be designed. Accordingly, the research should also focus on the statistical distribution of the fatigue limit to provide safe design methodologies.

To conclude, all the formulations analyzed in this section can be applied. The formulation in Equation 2 does not require a time-consuming experimental campaign and the following fractographic analysis. However, the validity of the assumed parameters and also the assumption on the size of the FGA should be verified on a larger number of experimental results. On the other

hand, formulations in Equations 4 and 7 require time-consuming experimental tests, and the FGA size must be necessarily measured. Therefore, they are surely valid for the tested material. In general, experimental tests on the material that will be used for the final component and a proper estimation of the material parameters involved in the models are recommended, rather than assuming averaged material parameters based on literature results.

3 | FATIGUE LIFE IN VHCF

In this section, the models for the VHCF life are investigated, focusing on those models that can be used for the estimation of the P-S-N curves, rather than on those aiming at estimating the fatigue life consumed in the crack initiation and propagation stages. For the sake of clarity, a classification based on the initial approach followed to define the stress-life relation (e.g., fitting of the data with a power-law relation, probabilistic approach, fracture mechanics approach, and integration of the Paris law) has been considered. It is worth noting that some of the investigated models combine different approaches: In this case, the models have been grouped depending on the prevalent approach.

First of all, the classification of the P-S-N curves covering the entire LCF-VHCF life range must be analyzed. Indeed, the S-N curves showing a first decreasing trend at high-stress amplitude (in the LCF and in HCF region), a plateau (corresponding to the conventional fatigue limit) and a second decreasing trend with failures originating from internal defects are called “step-wise S-N curves” or “duplex S-N curves.” In Section 3.1, the papers focusing on the classification of the S-N curves with the above-described trend are analyzed. Thereafter, the models developed in the literature have been analyzed. In Section 3.2, the models that enable to assess the stress-life relations in the VHCF life range by exploiting the Basquin law or a power law are analyzed. In Section 3.3, the models for the fatigue life or the P-S-N curves developed by assuming the statistical distribution of the fatigue life are analyzed and described (probabilistic approach). In Section 3.4, the models based on the fracture mechanics approach are, on the other hand, described. Section 3.5 focuses on models based on the integration of the Paris law. Finally, in Section 3.6, the results are summarized, focusing on the strengths and the weakness of the approaches followed and on considerations on the use of the analyzed models for the design of components.

The differences between the fatigue limit (Section 2) and the fatigue strength at a defined N_f which can be computed by assessing the stress-life relationship

(Section 3) are worth to be highlighted. Indeed, the models for the fatigue limit computed in Section 2 have the objective to assess the threshold for crack propagation, that is, the stress threshold below which a crack does not propagate, even if a defect is present or different weakening mechanisms²⁴ are present. On the other hand, the models described in Section 3 enable us to assess the stress-life relationship and, accordingly, the fatigue strength at a defined number of cycles to failure.

3.1 | Step-wise and duplex S-N curves: General classification

The experimental evidence that failures below the conventional fatigue limit (i.e., the asymptote in a S-N curve) may occur has made it necessary to revise the models conventionally used for defining the stress-life relation in an S-N plot, in order to include also the VHCF region. S-N curves characterized by a first decreasing trend at high-stress amplitude, a plateau (corresponding to the conventional fatigue limit and called in the following “transition stress”), and a second decreasing trend below the plateau are called in the literature “step-wise” or “duplex” S-N curves interchangeably. For example, in Nishijima and Kanazawa,⁴¹ these types of S-N curves are called step-wise S-N curves. The P-S-N curves at different failure probabilities in Nishijima and Kanazawa⁴¹ are obtained by fitting the experimental data through the application of a statistical method called probit analysis (in Hanaki et al.,⁴² the reader can find details on the application of the probit analysis to fatigue data). The paper⁴¹ is mainly focused on the comparison of the step-wise P-S-N curves obtained by testing different materials, and no details on the statistical distribution of the fatigue life and on the classification of the P-S-N curves are provided.

On the other hand, a more detailed classification of the S-N curves with the above-described trend is provided in Shiozawa and Lu.⁴³ According to Shiozawa and Lu, the terms “step wise” or “duplex” cannot be used interchangeably, since they refer to two different types of curves, even though with a similar shape. Shiozawa and Lu proposed a classification based on the statistical distribution of the fatigue life associated with the first failure mode in the LCF-HCF region (surface failure mode) and the statistical distribution of the fatigue life associated with the second failure mode (internal failure mode). Figure 5 shows the classification for the P-S-N curves proposed in Shiozawa and Lu,⁴³ which is based on the experimental evidence that the fatigue life distributions associated with the surface failure mode and with the internal failure mode are different.

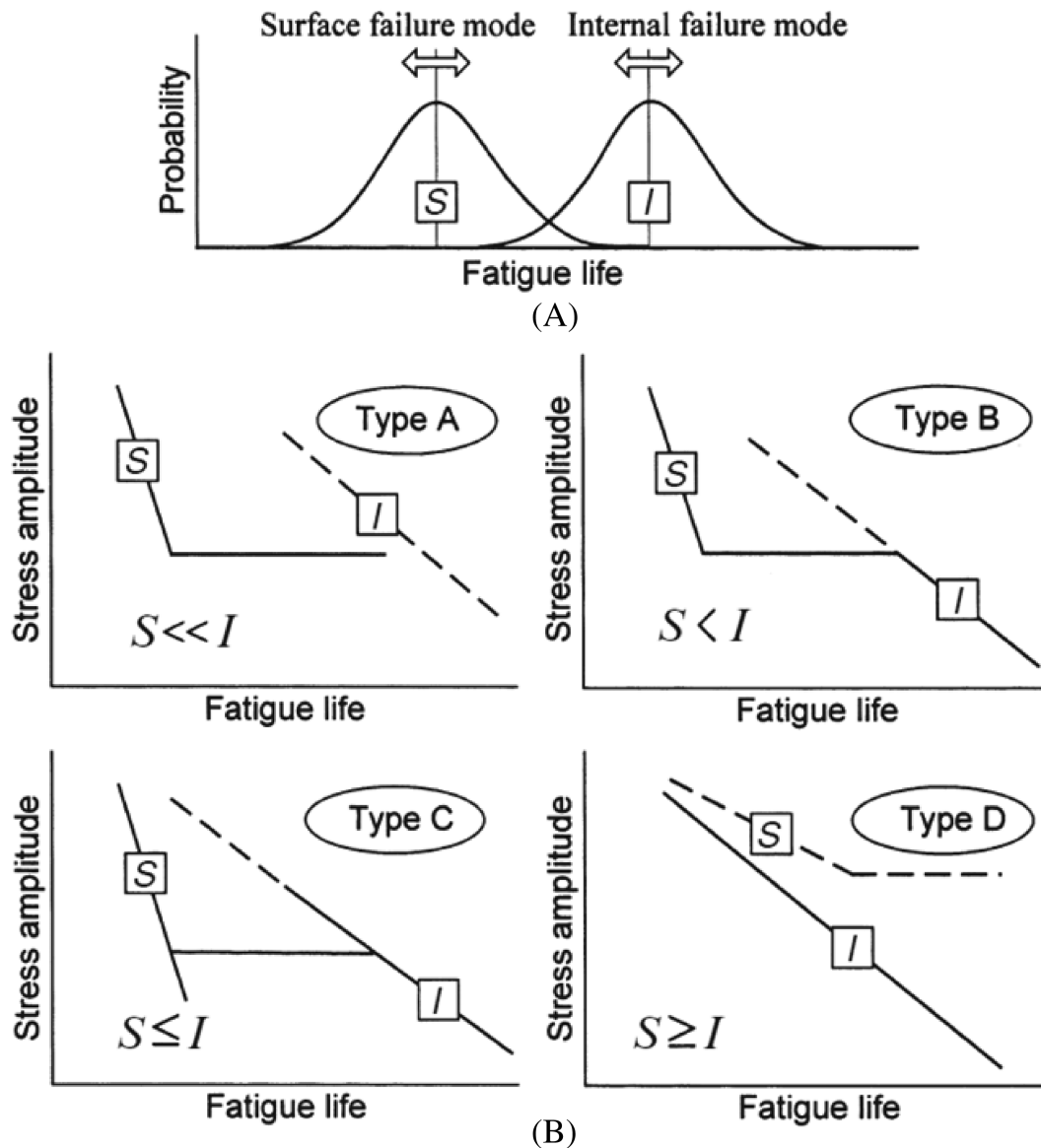


FIGURE 5 Classification of the S-N curves including the VHCF region in I^{43} (reprinted with permission from Wiley)

According to the Shiozawa and Lu, “Type A” is the S-N curve of low-carbon steels (no internal failures); “Type B” is the typical “step-wise S-N curve,” since the probability distributions for the surface and the internal failure modes do not overlap. On the other hand, “Type C” curve is the typical “duplex S-N curve,” since surface failures and internal failures partially overlap for stress amplitude close to the transition stress. Finally, “Type D” is the S-N curve of materials failing due to only internal defects (no surface failures, even in the HCF region). Accordingly, Shiozawa and Lu clearly distinguish between step-wise and duplex P-S-N curves.

In Mughrabi,^{3,4} the duplex P-S-N curves are further described, focusing on the mechanisms of crack initiation. Sakai et al.⁶ recommend the expression “duplex S-N curves” instead of “two-step S-N curve” or “doubly

reflected S-N curve” if two failure modes are present. In our opinion, “duplex P-S-N curves” is more appropriate for the S-N curves including also the VHCF region, since, in the proximity of the transition stress, the fatigue failure can originate both from the specimen surface or from internal defects, without a clear separation between the two failure modes.

It is worth noting that S-N curves with different trends have also been found in the literature, like the S-N curves with a double slope without a plateau between the two failure modes^{44,45} For a detailed classification, the reader could refer to Sonsino.⁴⁴ However, a transition stress between the two failure modes is generally found experimentally when the VHCF region is also analyzed, thus justifying the importance of the classification in Shiozawa and Lu.⁴³

3.2 | VHCF life range: Fitting with the power law

In this section, the power-law is exploited to assess the S–N curves in the VHCF life range. It represents the simplest approach, with a linear decreasing relationship between s_a and N_f in the VHCF region. All the models analyzed in this section focus only on the VHCF life range.

For example, in Akiniwa et al.,⁴⁶ the P–S–N curves for specimens subjected to axial and torsional loads have been estimated by assuming a power-law dependency between the applied stress amplitude (axial or torsional) and the number of cycles to failure. The power law was found to be in good agreement with the experimental data for both the load types. Figure 6A,B shows the experimental data (obtained by testing oil-tempered Si–Cr steel wire used for valve springs, JIS G3561, SWOSC–V) and the estimated S–N curves on the S–N plot for axial and torsional loads, respectively. The median curves are shown, together with, according to the authors, the 90% confidence interval, even though the two bounds of the confidence interval seem to correspond to the 5th and the 95th quantiles curves.

A similar approach based on the power law has been followed in Liu et al.²⁹ In particular, the paper focused on the procedure for the estimation of the parameters involved in the power-law equation ($s_a = \sigma_f' \cdot (2 \cdot N_f)^b$), being σ_f' and b two constant coefficients to be estimated from the experimental data. Indeed, the methodology developed for the assessment of the fatigue limit in the presence of defects and with FGA formation^{28,35} is exploited also for the estimation of the P–S–N curves. In particular, an expression for the fatigue limit from defects

(i.e., without the formation of the FGA) in the HCF region, $s_{i,LIU,H}$, is obtained. The two constant coefficients involved in the Basquin equation, σ_f' and b , are therefore estimated by supposing that for $N_f = 10^6$ cycles, $s_a = s_{i,LIU,H}$ and that for $N_f = 10^9$ cycles, $s_a = s_l$, being s_l the fatigue limit computed according to Equation 4. The proposed model has been validated on experimental datasets obtained by the authors through ultrasonic fully reversed tension–compression fatigue tests on spring steels and available in the literature. Figure 7 plots the estimated model and the experimental data in an S–N plot. The S–N curve estimated with other literature models^{34,47,48} is also shown in Figure 7 (“Chapetti” in the figure is the model in Chapetti et al.,³⁴ “Mayer” is the model in Mayer et al.,⁴⁸ and “Tanaka” is the model in Tanaka and Akiniwa⁴⁷). The two bounds represent the curves estimated from the largest and the smallest defect size. The authors conclude that the proposed formulation permits obtaining a good fit of the data. No indications on the fatigue life statistical distribution are provided.

In Wang et al.,⁴⁹ a three-parameter model is considered for fitting the experimental data. Differently from the previous analyzed model, a three-parameter model involves an asymptotic trend at the end of the curve:

$$(s_a - s_{0,R})^{\alpha_R} \cdot N_f = C_R, \quad (10)$$

being $s_{0,R}$, α_R , and C_R material parameters to be estimated from the experimental data. Moreover, the fatigue life is considered normally distributed in order to model the scatter associated to the experimental data. The model has been validated on an experimental dataset obtained by testing a high-strength martensitic stainless steel FV520B-I, but the paper is mainly focused on their

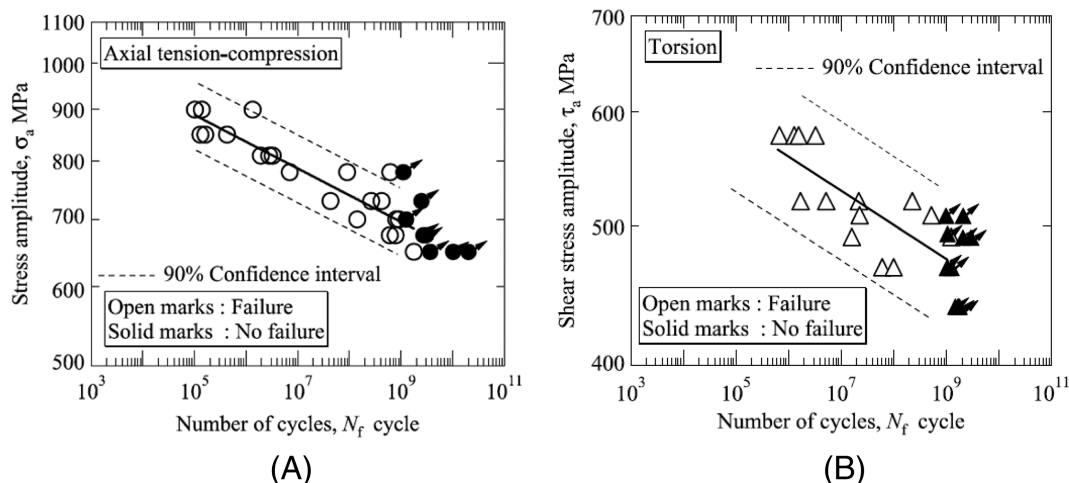


FIGURE 6 Validation of the model for the VHCF life in Akiniwa et al.⁴⁶: (A) S–N plot for specimens subjected to axial load and (B) S–N plot (shear stress amplitude τ_a with respect to N_f) for specimens subjected to torsional load (reprinted with permission from Elsevier)

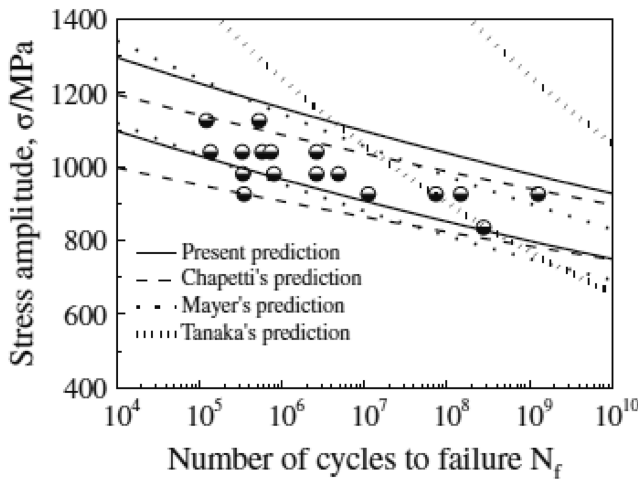


FIGURE 7 Validation of the model for the VHCF life in Liu et al.²⁹: S–N plot with the proposed model and literature models (reprinted with permission from Elsevier)

analysis on the estimation of the relation between the defect size and N_f .

Sun et al.²⁷ analyzed a dataset obtained by testing through ultrasonic fully reversed tension–compression tests a high-carbon–chromium steel and interestingly showed that s_a , N_f , and $a_{d,0}$ can be correlated with the following equation:

$$s_a = C \cdot N_f^l \cdot a_{d,0}^m, \quad (11)$$

being C , l , and m material parameters. Equation 11, therefore, models the dependence of the fatigue life on the defect size and can therefore be employed for the assessment of the P–S–N curve for VHCF failures originating from defects. The parameters have to be estimated from the experimental data, since they may vary depending on the material or on the heat treatment. The model has been validated on the datasets obtained by the authors (high-carbon–chromium steel) and on literature datasets obtained through rotating bending fatigue tests at $R = -1$ and axial fatigue tests at $R = -1$. Figure 8A,B show the proposed model and literature data on an S–N plot, for rotating bending fatigue tests and axial loading fatigue tests, respectively.

The model has been also modified to take into account the influence of the stress ratio of the VHCF response. Starting from Equation 11 and by considering previous results, the influence of the stress ratio can be expressed as follows:

$$s_a = C \cdot N_f^l \cdot a_{d,0}^m \cdot \left(\frac{1-R}{2} \right)^\alpha, \quad (12)$$

being α an unknown material parameter to be estimated from the experimental data. The model has been validated on literature datasets obtained by testing high-strength steels at different stress ratios (Figure 8C). The model was found to be in agreement with experimental data, proving to be capable to assess the influence of the stress ratio. In the paper, the authors moreover proposed to assess the largest defect expected in the risk volume with the Gumbel distribution.

In Mayer et al.,⁴⁸ the Basquin model is exploited to take into account also the dependence between the defect size and the fatigue life, too. In particular, a bainitic high-carbon–chromium steel is subjected to ultrasonic fully reversed tension–compression tests, and surface and internal failures are found in the HCF and in the VHCF region, respectively. Moreover, the authors found that the experimental data plotted in a $s_a \cdot (\sqrt{a_{d,0}})^{\frac{1}{2}}$ versus N_f diagram show a smaller scatter than the one found by reporting the experimental data in a traditional S–N plot, due to the influence of the defect size on the fatigue life. Accordingly, the dependency between N_f , s_a , and $\sqrt{a_{d,0}}$ is expressed by the authors as

$$\left(s_a \cdot (\sqrt{a_{d,0}})^{\frac{1}{2}} \right)^n \cdot N_f = C, \quad (13)$$

being n and C two material parameters. The experimental failures originating from defects in the VHCF region and the estimated model (i.e., the median curve) are shown in Figure 9.

The same research group adopted a similar approach in Schönbauer et al.⁵⁰ The VHCF response of a 17-4PH steel subjected to variable amplitude loads is experimentally investigated, focusing also on the influence of the load ratio. It was also found that the stress ratio R has a strong influence on the fatigue life of specimens subjected to loads with constant amplitude (CA) and variable amplitude (VA) and it was proposed to normalize and condense the experimental data by replacing the stress amplitude with the following equivalent stress s_{eq} in an S–N plot ($s_{eq,CA}$ for CA and $s_{eq,max,VA}$ for VA):

$$s_{eq,CA} = \frac{s_a}{\left(\frac{1-R}{2} \right)^\alpha}, \quad (14)$$

and for VA loads,

$$s_{eq,max,VA} = \frac{s_{a,max}}{\left(\frac{1-R}{2} \right)^\alpha}, \quad (15)$$

being α a constant coefficient. This relation has been obtained by considering the Murakami model,³⁰ and the coefficient α is obtained through a fitting of the

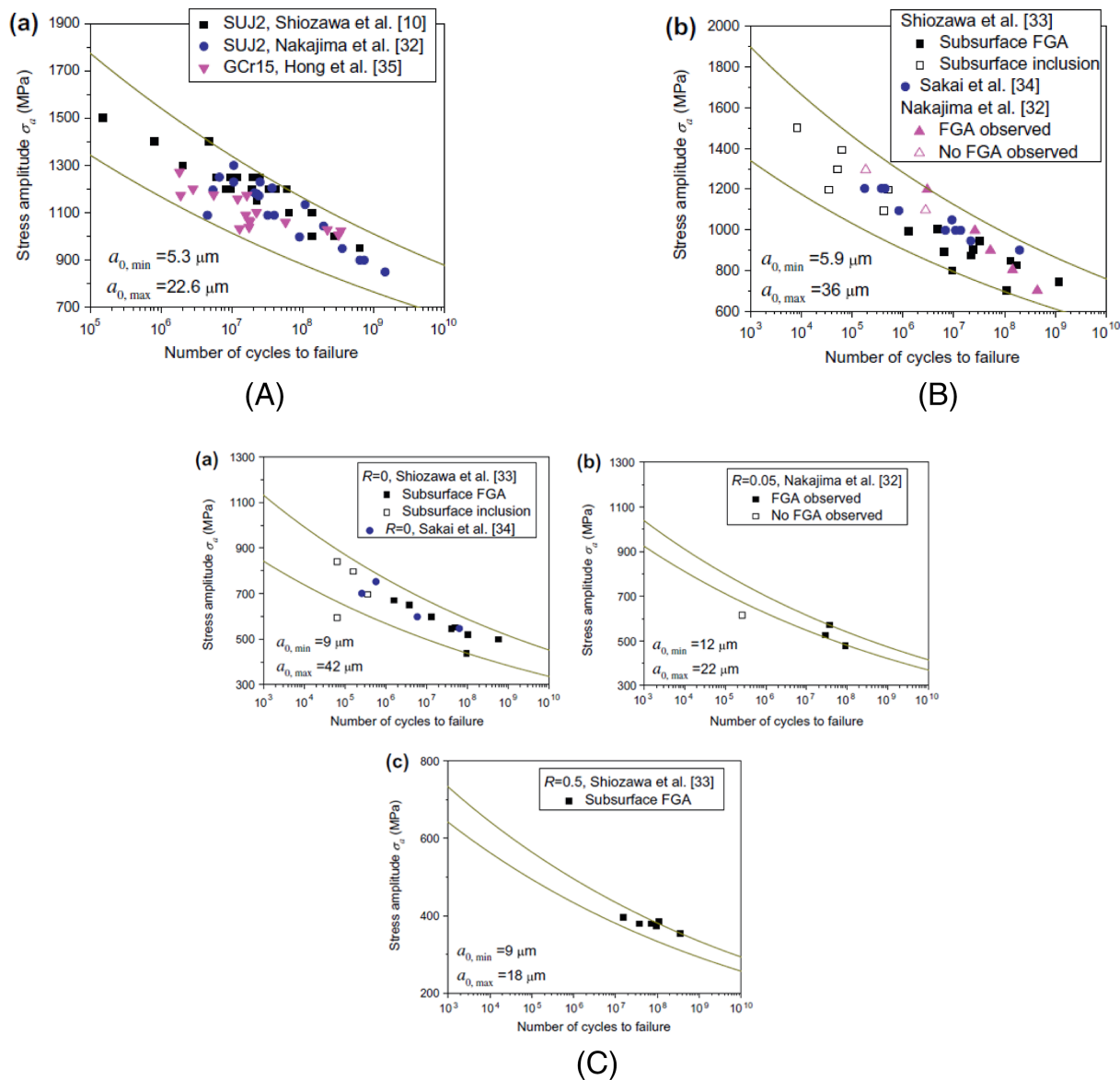


FIGURE 8 Validation of the model for the VHCF life in Sun et al.²⁷: (A) experimental data and estimated model on an S–N plot for literature datasets obtained through rotating bending tests. (B) Experimental data and estimated model on an S–N plot for literature datasets obtained through axial tests. (C) Validation of the model in Equation 12 that models the effect of the stress ratio R (reprinted with permission from Elsevier) [Colour figure can be viewed at wileyonlinelibrary.com]

experimental results in Schönbauer et al.⁵¹ Figure 10A,B shows the experimental data in $S_{eq,CA}-N_f$ and $S_{eq,max,VA}-N_f$ plots and the estimated models, respectively. In Figure 10, σ_a corresponds to s_a . The scatter associated to the experimental data and the statistical distribution of the fatigue life is not discussed.

According to the models analyzed in this section, the power law is effective also in modeling the fatigue life and, accordingly, the P–S–N curves in the VHCF life range. The models have been validated mainly on high-strength steels, and no validation on other materials can be found. Moreover, and this could be the most critical issue, all these models fail to take into account the scatter

associated to the experimental failure, which is, on the contrary, fundamental from a design point of view. On the other hand, in Akiniwa et al.,⁴⁶ the Basquin model has been considered for analyzing the results of torsion tests: This is the unique validation available in the literature on loads different from tension–compression loads. Moreover, modifying the power law in order to take into account the defect size proved to be an effective strategy (Sun et al.²⁷ and Mayer et al.⁴⁸), also in reducing the scatter associated to the experimental data on an S–N plot (Mayer et al.⁴⁸). The influence of the stress ratio has also been investigated, following an approach based on the Murakami model.^{27,48} An asymptotic behavior, on the

other hand, is not considered in the analyzed models, apart from Wang et al.⁴⁹ However, this assumption must be verified.

To conclude, the adoption of a power-law model for the S–N curves in the VHCF life range has proved to be effective. This model is simple, and the procedure for parameter estimation is not complex, too. By appropriately modifying the original model, moreover, it has been shown that the dependence between the fatigue life and the defect size or the stress ratio can be assessed. However, the randomness associated with the experimental

data was not considered in most of the models: This limitation can prevent their adoption for practical applications. On the other hand, the model in Sun et al.²⁷ is the most general, since it permits modeling both the influence of inclusion size and the stress ratio, enabling also to estimate the curves at different $a_{d,0}$.

3.3 | Models for the S–N curves: Probabilistic approach

In this section, the models for the stress–strain relation based on a “probabilistic approach” are analyzed in detail. According to this approach, the statistical distribution of the fatigue life is a priori assumed, with the main aim of estimating the P–S–N curves. As discussed in detail the following, a log-normal distribution or a Weibull distribution for the fatigue life have proved to be effective even for the VHCF region. For the sake of clarity, in Section 3.3.1, the models for the stress–life relation that considers only the VHCF region, for example, the region below the fatigue limit for high-strength steels, are analyzed. On the other hand, the models dealing with the LCF–VHCF life range are described in detail in Section 3.3.2.

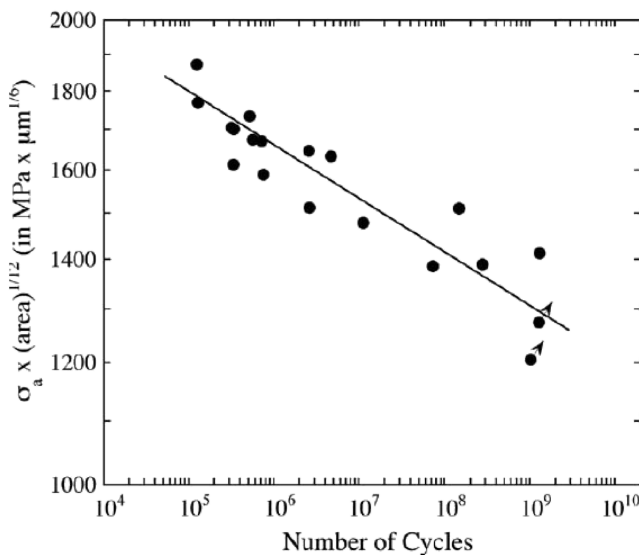


FIGURE 9 Validation of the model for the VHCF life in Mayer et al.⁴⁸: S–N plot with normalized stress amplitude (reprinted with permission from Elsevier)

3.3.1 | VHCF life range: Probabilistic approach

In this section, the models focusing only on the VHCF life range are described. The statistical distribution of the fatigue life is assumed to properly fit the experimental

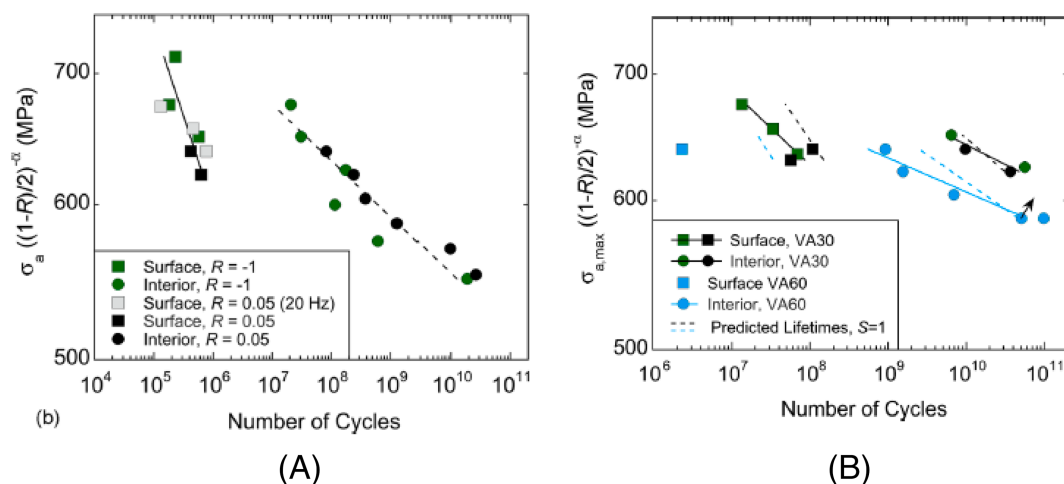


FIGURE 10 Validation of the model for the VHCF life in Schönbauer et al.⁵⁰: (A) experimental data and estimated model on a $S_{eq,CA}$ with respect to N_f . (B) Experimental data and estimated model on a $S_{eq,max,VA}$ with respect to N_f (reprinted with permission from Elsevier) [Colour figure can be viewed at wileyonlinelibrary.com]

data. It is worth noting that, if the entire LCF–VHCF life range is considered, the models analyzed in this section can be combined with traditional models (e.g., the Basquin law, the staircase method) for the LCF–HCF life range. However, the continuity and a smooth transition between the LCF–HCF life range and the VHCF life range is, obviously, not guaranteed.

A first probabilistic method for the prediction of the VHCF fatigue life is proposed in Chantier et al.⁵² The model is based on the probability of finding a defect with critical size and on the weakest link approach. A method for extrapolating the fatigue life starting from the tests carried out up to 10^7 cycles is proposed, but the S–N curves in the VHCF region are not estimated. A similar approach based on the weakest link approach has been used in many other subsequent models: For this reason, this paper is worth to be cited.

In Paolino et al.,^{36,37} the dependence between the defect size and the fatigue life is modeled in a probabilistic framework. The curve ends with an asymptotic trend, that is, a fatigue limit. The finite VHCF fatigue life has been assumed to be log-normally distributed, with the mean $\mu_{Y|int}$, assumed to be dependent not only on the logarithm of the applied stress amplitude (i.e., Basquin relation) but also on the defect size ($\mu_{Y|int} = c_Y + m_Y \cdot \log_{10}(s_a) + n_Y \cdot \log_{10}(\sqrt{a_{d,0}})$, being c_Y , m_Y , and n_Y constant material coefficients to be estimated from the experimental data). From this model and by considering the formulation for the fatigue limit described in Section 2 and in Equation 8, the “conditional P–S–N curves,” that is, the P–S–N curves conditioned to the defect size (the P–S–N curve for a specific defect with size $\sqrt{a_{d,0}}$), can be obtained, according to Equation (16):

$$F_{Y|\sqrt{a_{d,0}}}(y; x, \sqrt{a_{d,0}}) = \Phi\left(\frac{y - \mu_{Y|int}(x, \sqrt{a_{d,0}})}{\sigma_Y}\right) \cdot \Phi\left(\frac{x_l - \mu_{X_l}(\sqrt{a_{d,0}})}{\sigma_{X_l}}\right), \quad (16)$$

being $\Phi\left(\frac{y - \mu_{Y|int}(x, \sqrt{a_{d,0}})}{\sigma_Y}\right)$ the cdf of the conditional finite fatigue life and $\Phi\left(\frac{x_l - \mu_{X_l}(\sqrt{a_{d,0}})}{\sigma_{X_l}}\right)$ the cdf of the conditional fatigue limit, according to Equation 8. Equation 16 enables to model the dependence between the fatigue life and the defect size and also the statistical scatter associated to the experimental data. The model involves a linear decreasing trend, ending with an asymptote. However, for the experimental data that do not show a clear fatigue limit, a continuous decreasing trend can be also modeled by considering $\Phi\left(\frac{x_l - \mu_{X_l}(\sqrt{a_{d,0}})}{\sigma_{X_l}}\right) = 1$.

The same research group, moreover, proposed a second type of P–S–N curves, the so-called marginal P–S–N curves, i.e., the P–S–N curves obtained by exploiting the definition of “marginal distribution,” which enable to assess the stress–life relation independently of the defect size. The marginal P–S–N curves are estimated by considering the conditional distribution of the fatigue life and the statistical distribution of the defect size rv, $\sqrt{A_{d,0}}$, which is assumed to follow a LEVD, with final formulation:

$$F_{Y|int}(y; x) = \int_0^\infty F_{Y|\sqrt{a_{d,0}}}(y; x, \sqrt{a_{d,0}}) f_{\sqrt{A_{d,0}}}(\sqrt{a_{d,0}}) d\sqrt{a_{d,0}}, \quad (17)$$

being $F_{Y|int}(y; x)$ the cdf of the marginal distribution of the fatigue life (i.e., dependent only on $x = \log_{10}(s_a)$), $F_{Y|\sqrt{a_{d,0}}}(y; x, \sqrt{a_{d,0}})$ the cdf of the conditional fatigue life and $f_{\sqrt{A_{d,0}}}$ the probability density function (pdf) of $\sqrt{a_{d,0}}$, assumed to follow a LEVD. The procedure for parameter estimation, based on the analysis of the fracture surfaces and requiring the measurement of the defect and the FGA size, is detailed in Paolino et al.³⁶ In particular, the unknown parameters for the fatigue limit are estimated by maximizing the likelihood function associated to the probability of having a failure or a runout for the experimental data (Section 2), whereas the unknown parameters for the finite VHCF life are estimated through a multiple linear regression. The model in Equation 17 has been validated on an experimental dataset obtained by the authors through ultrasonic tension–compression tests on H13 steels in the VHCF region. Figure 11 shows the estimated marginal P–S–N curves, together with the experimental data and the estimated model.

In Qian et al.⁵³ and Wu et al.,⁵⁴ a different approach is followed to assess the stress–life relation, even if the P–S–N curves are finally not estimated. However, they present innovative aspects, and therefore, they are worth to be mentioned and briefly recalled.

In Qian et al.,⁵³ a model for the prediction of the S–N curves of specimens tested in different environmental media is obtained through an energetic approach. In particular, the number of cycles necessary for a crack initiation from a subsurface defect is computed by considering the surface energy related to crack initiation and the grain radius. The model is exploited to assess the influence of the environment media, of the mechanical properties and of the defect size on the HCF and VHCF response. However, according to the authors, “the proposed model ‘qualitatively’ predicts S–N curves for surface and subsurface crack initiation in different environmental

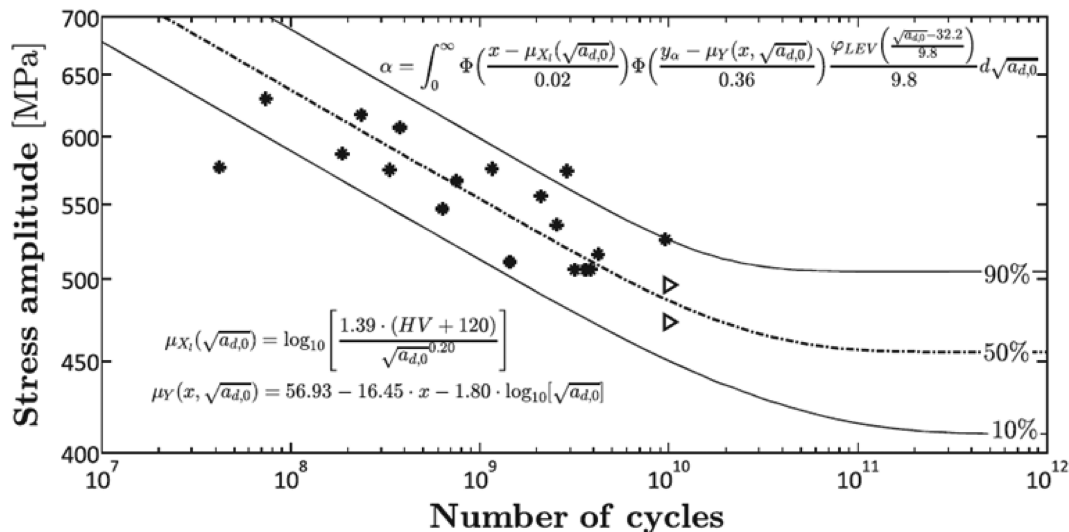


FIGURE 11 Validation of the model for the VHCF life in Paolino et al.³⁶: P-S-N and experimental data (reprinted with permission from Wiley)

media, but a procedure for estimation is not provided and considered as a further development.”

In Wu et al.,⁵⁴ the VHCF response of a braided carbon fiber-reinforced plastic (CFRP) composite is experimentally assessed. The fatigue life distribution is obtained by considering the crack density distribution and by considering a “matrix crack density” damage as the mechanism for failures in the investigated composite material. A three-parameter model has been considered for modeling the matrix crack density life damage evolution (“The crack density increases with the number of cycles under all loading conditions, and the increasing speed of crack density lowers down with the increase of cycles”), whose parameters are estimated from the experimental VHCF tests. The VHCF response has been thereafter predicted and a strain threshold computed, i.e., the strain amplitude below which no damage occurs even in the VHCF region. The distribution of the fatigue life is obtained by equaling the fatigue life distribution function and the crack density distribution function, which controls the fatigue damage. The damage distribution model of matrix crack density is assumed to follow a bimodal Weibull distribution (i.e., two morphologies of matrix crack density are assumed). The probability density function of the fatigue life has been finally compared with the experimental data, but the relation between the applied stress and the fatigue life is not assessed.

According to the models analyzed in this section, the normal distribution is assumed for VHCF fatigue life distribution, as in the LCF-HCF life range. The model described in Paolino et al.³⁶ enables to assess the dependence between the fatigue life and the defect size and to model the mechanisms for the FGA formation. It

requires a detailed analysis of the fracture surfaces to assess the defect size and the FGA size. Accordingly, it can be applied only if, for each experimental failure, s_a , $\sqrt{a_{d,0}}$ and N_f are available or can be reliably measured. The model is valid for all VHCF failures originating from defects with or without FGA formation: For example, it has been used for the assessment of the P-S-N curves for an AlSi10Mg alloy produced through an additive manufacturing process.⁵⁵ For the VHCF life range, only one model that permits estimating the P-S-N curves has been found: Indeed, other models for the fatigue life in VHCF are estimated through a fracture mechanics approach, a mixed probabilistic/fracture mechanics approach, or consider also the LCF-HCF life range, as detailed in the following subsection.

3.3.2 | LCF-VHCF life range and duplex P-S-N curves: Probabilistic approach

In this section, the models for the fatigue life in the LCF-VHCF life range are described. Most of the models focused on the presence of two failure modes, according to the experimental evidence. The presence of a transition stress or of a knee point is another characteristic of the models analyzed in this section.

Sonsino⁴⁴ investigated the shape of the P-S-N curves by analyzing literature datasets and by considering a bilinear model with a “knee point.” Different metallic materials have been considered; the parameters have been estimated through a linear regression, to show that the continuous decrease of the fatigue strength in the VHCF region reduces the safety against failures and the

effectiveness of a design based on the fatigue limit concept. However, a procedure for the estimation of the P-S-N curve is not proposed.

In Weixing and Shenjie,⁵⁶ the fatigue life in the presence of two failure modes (surface and internal failure modes) has been modeled in a statistical framework, by assuming that the fatigue life distribution has a double-peaked shape. The cdf of the fatigue life, $F(x)$, is obtained as the weighted sum of the cdfs, $F_1(x)$ and $F_2(x)$, associated with the first and the second failure modes, respectively, and with t as the weighting coefficient:

$$F(x) = t \cdot F_1(x) + (1 - t)F_2(x). \quad (18)$$

The fatigue life is assumed to follow a log-normal distribution. A procedure for the estimation of the unknown parameters is provided, and the model is validated on an experimental dataset obtained by testing the aluminum alloy LC4CS. Figure 12 plots the probability $F(x)$ with respect to the number of cycles to failure. No indications on the estimation of the P-S-N curves are provided.

Zhao et al.⁵⁷ analyzed the experimental data with standard codes (AASHTO standard⁵⁸ and ECCS code⁵⁹), showing that they are not effective in estimating the P-S-N curves, especially if the VHCF region is also considered. An innovative model is, therefore, defined: The fatigue life r_v is assumed to follow a log-normal distribution, with the mean and standard deviation linearly dependent on the applied stress amplitude and with the stress-life in the HCF region and in the VHCF region modeled with a power law. A formulation for the P-S-N curves in the HCF region is provided, with the unknown material parameters estimated through the application of the maximum likelihood principle. The unknown

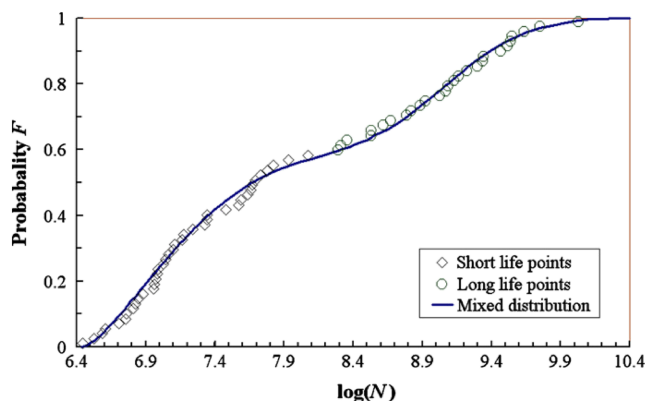


FIGURE 12 Validation of the model for the VHCF life in Weixing and Shenjie⁵⁶: cdf of the fatigue life, $F(x)$, with respect to N_f (reprinted with permission from Wiley) [Colour figure can be viewed at wileyonlinelibrary.com]

material parameters of the model for the VHCF life are obtained through a probabilistic concurrent model, according to the relation shown in Figure 13A. The distribution of the fatigue life in the VHCF region is thereafter obtained and the procedure for the parameter estimation is provided, with the final S-N curves characterized by a bilinear shape with a transition point, N_T . N_L represents the fatigue life, according to the authors. The model has been validated on a dataset obtained by testing the LZ50 axle steel, as shown in the S-N plot in Figure 13B. According to the authors, the proposed model is in agreement with the experimental data, with the 0.999th quantile P-S-N curve below all the experimental failures. The Student's t -distribution is considered for estimating the quantiles of the S-N curves.

It must be noted, however, that for the analyzed dataset, only one failure occurred at N_f above 10^8 cycles. Moreover, the origin of the fatigue failures in HCF and in VHCF is not investigated, and the presence of two failure modes is not modeled. Therefore, this model can be applied depending on the experimental dataset, i.e., it would not be appropriate for datasets showing a transition stress with a plateau and to model the influence of defects, if failures in VHCF originate from defects.

In Sakai et al.,⁶ the fatigue life is assumed to follow a Weibull distribution. The occurrence of two failure modes is also modeled. The experimental data obtained by testing a high-carbon-chromium steel for bearings (JIS Material Code: SUJ2) showed two failure modes: surface failures for high-stress levels and internal failures for low-stress levels, with fish-eye morphology. Accordingly, two distinct statistical distributions are considered for the fatigue life associated to surface and internal failures. For each investigated stress level, the distribution of the fatigue life is estimated, thus enabling to assess the P-S-N curves. Moreover, a mixed-mode Weibull distribution ($F = p_1 \cdot F_1(N_f) + p_2 \cdot F_2(N_f)$, being F_1 and F_2 the cdfs of the fatigue lives and p_1 and p_2 the occurrence probability, with the subscript 1 and 2 referring to the first and the second failure mode, respectively) is considered for modeling the occurrence of two failure modes. The occurrence probabilities, p_1 and p_2 , are estimated by analyzing the experimental data close to the transition stress ("At medium stress levels, the occurrence probability of each fracture mode is determined by the occurrence frequencies of the respective fracture modes"), showing that p_1 tends to increase with the applied stress and p_2 tends to increase as the applied stress is decreased. The proposed model has been validated on the experimental data obtained by the authors. Figure 14A shows the Weibull plots of the fatigue life distribution, with the dashed line indicating the conventional Weibull distribution and the

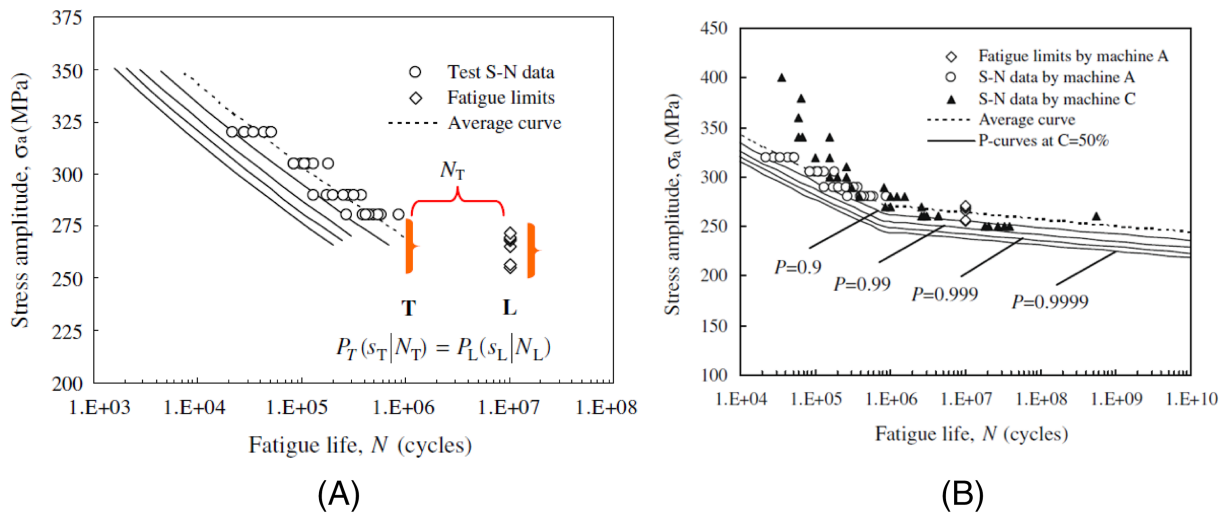


FIGURE 13 Validation of the model for the VHCF life in Zhao et al.⁵⁷: (A) concurrent probabilistic model for estimating the S-N curves in the VHCF region and (B) experimental data and estimated model on an S-N plot (reprinted with permission from Elsevier) [Colour figure can be viewed at wileyonlinelibrary.com]

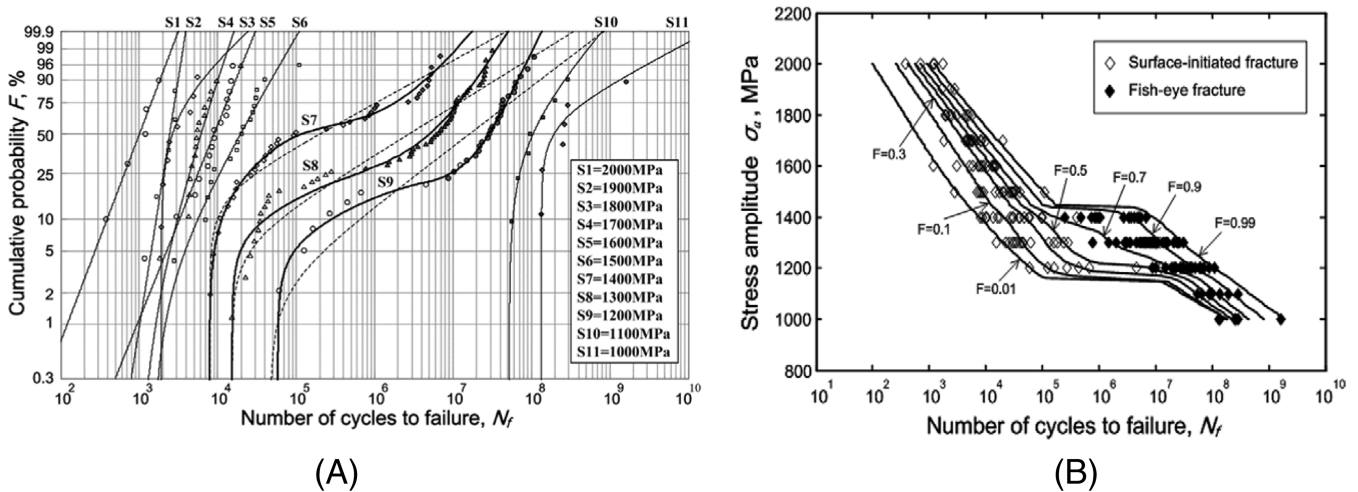


FIGURE 14 Validation of the model for the VHCF life in Sakai et al.⁶: (A) Weibull plots of the fatigue life distribution and (B) experimental data and estimated P-S-N curves (reprinted with permission from Elsevier)

solid line the mixed-mode Weibull distribution. Figure 14B plots the estimated duplex P-S-N curves, confirming the effectiveness of the proposed model. The authors concluded by pointing out that the presence of a VHCF fatigue limit at 10^{10} cycles is still debated in the literature and cannot be assumed, since it has to be experimentally verified.

In Bomas et al.,⁶⁰ a different approach is proposed, and the fatigue life distribution function is computed by assuming that the probability of crack initiation due to a specific mechanism is independent from the probability of failure due to a different failure mechanism. In general, according to Bomas et al.,⁶⁰ the cdf of the fatigue life, $F(N_f, s_a)$, can be expressed as follows:

$$F(N_f, s_a) = 1 - \prod_{i=1}^{n_{th}} (1 - F_i(N_f, s_a)), \quad (19)$$

being n_{th} the number of failure modes ($i = 1, \dots, n_{th}$) and $F_i(N_f, s_a)$ the cdf of the fatigue life associated to the i -th failure mode, expressing the probability of having a failure at a number of cycles smaller than N_f for an applied stress amplitude equal to s_a . The fatigue life rv is assumed to follow a two parameters Weibull distribution, and a procedure for the estimation of the constant coefficients, according to the Stepanov method,⁴⁷ is provided. The model has been validated on experimental data obtained by testing notched specimens made of the

carburized, quenched and tempered steel SAE 5115 (DIN 20MnCr5). As shown in Figure 15, the model has been validated by considering only the median S-N curve, even if the model in Equation 19 enables to assess also the quantiles of the P-S-N curves. Further validations are therefore required to confirm the effectiveness of the proposed model.

In Li et al.,⁶¹ the model in Bomas et al.⁶⁰ has been further developed and validated on an experimental dataset obtained by testing a carburized Cr-Mn-Si steel. Three failure modes are found experimentally: surface flaw-induced failure at high-stress amplitude (first failure mode, I), interior inclusion-induced failure without the FGA (second failure mode, II), and interior inclusion-induced failure with the FGA at low-stress amplitude (third failure mode, III). For each failure mode, the fatigue life is shown to be well described by a two parameters Weibull distribution function. In order to model the dependency between the fatigue life and the applied stress amplitude, the “characteristic life parameter” of the distribution of each failure mode is modeled with a three-parameter power equation for the first two failure modes (i.e., involving a linear decreasing trend with an asymptote) and with a Basquin equation for the third failure mode (involving only a linear decreasing trend). Indeed, the transition between the first and the second failure mode is the fatigue limit for first failure mode. Similarly, the transition from the second to the third failure mode is the fatigue limit for the second failure mode. The final model for the cdf of the fatigue life, $F(N_f, s_a)$, is given by Equation 20:

$$F(N_f, s_a) = 1 - \exp$$

$$\left[- \left(\sum_{j=I}^{II} \left(\frac{N_f}{(\sigma_{f,j}/(s_a - \sigma_{0j}))^{c_j}} \right)^{a_j + b_j s_a} + \left(\frac{N_f}{(\sigma_{f,III}/(s_a))^{c_{III}}} \right)^{a_{III} + b_{III} s_a} \right) \right], \quad (20)$$

being a_j , b_j , c_j , a_{III} , b_{III} , c_{III} , $\sigma_{f,j}$, σ_{0j} , and $\sigma_{f,III}$ material parameters estimated by considering the experimental failures at stress levels at which two of the three failure modes coexist (i.e., at the transition from one failure mode to the following one) and through a linear interpolation of the experimental data. The P-S-N curves at different failure probabilities are finally estimated and found to be in good agreement with the experimental data, especially for failure modes I and II, as shown in Figure 16A.

In Li et al.,⁶² the same research group has analyzed the experimental results of tests on specimens subjected to axial load. Differently from rotating bending tests, the authors point out that “the duplex S-N characteristics of bearing steel was not so distinct” due to the uniformity of stress distribution within the cross-section. A mixed Weibull distribution function has therefore been proposed to model the fatigue life in case of multiple failure modes and of axial loads (i.e., $F(N_f) = \sum_{i=1}^j P_i \cdot F_i(N_f)$, being j the total number of failure modes and $F_i(N_f)$ the three parameters Weibull distribution associated to the i -th failure mode). A method for the optimization of the parameters involved in the model has been also proposed and applied to estimate the P-S-N curves of the tested bearing steel SUJ2. The estimated P-S-N curves at different failure probabilities are shown in Figure 16B, proving that a “duplex behavior” with a transition stress between the two failure modes is not evident from the experimental data and that, despite this, the proposed model is effective for the analysis of the results of axial tests.

The properties of the Weibull distribution have been also exploited in Muniz-Calvente et al.⁶³ to estimate the P-S-N curves. In particular, a methodology for modeling the fatigue life in the HCF region, with failures originating from the specimen surface, and in the VHCF region, with failures originating from internal defects, is proposed and validated on experimental and simulated datasets. It involves different steps: The first step is the experimental activity, where the applied stress, the number of cycles, and the type of failure associated to each specimen are recorded. Thereafter, the distributions of the fatigue life for surface failures and for internal failures are estimated independently, by assuming for the fatigue life associated to each failure mode a Weibull distribution, according to the Castillo-Canteli model⁶⁴:

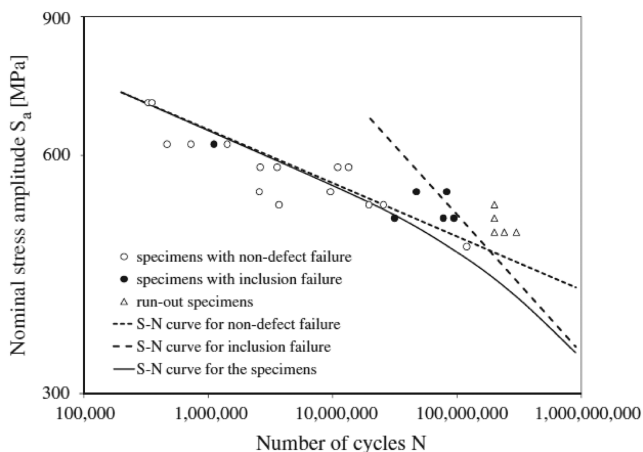


FIGURE 15 Validation of the model for the VHCF life in Bomas et al.⁶⁰: (A) S-N plot with the proposed model and experimental data (reprinted with permission from Elsevier)

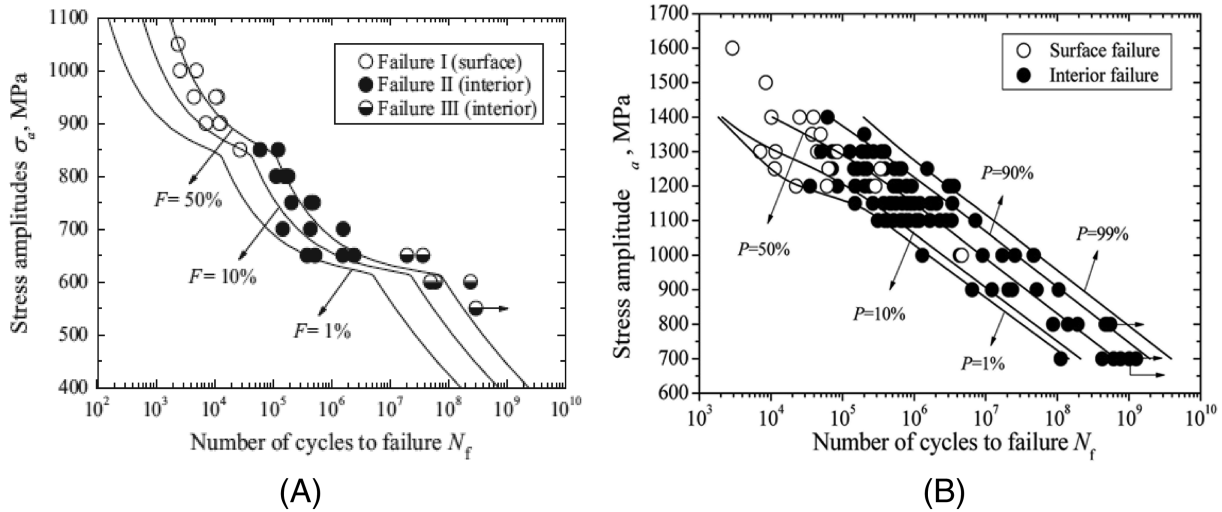


FIGURE 16 Validation of the model for the VHCF life in Li et al.^{61,62}: (A) S-N plot in Li et al.,⁶¹ with results obtained by carrying out rotating bending tests (reprinted with permission from Elsevier) and (B) S-N plot in Li et al.,⁶² with results obtained by carrying out axial tests (reprinted with permission from Taylor & Francis Online)

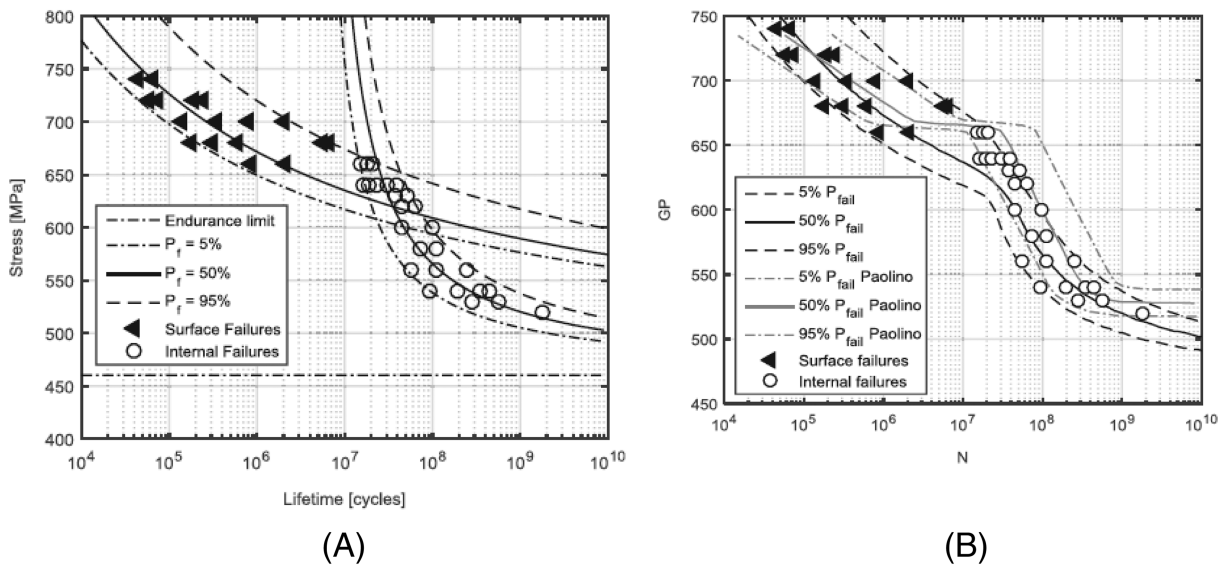


FIGURE 17 Validation of the model for the VHCF life in Muniz-Calvente et al.⁶³: (A) P-S-N curve estimated by considering the surface failure mode and the internal failure mode separately and (B) “combined P-S-N curve” (reprinted with permission from Wiley)

$$F(N_f; GP) = 1 - \exp \left[- \left(\frac{(\log(N_f) - B) \cdot (\log(GP) - C)}{\delta} \right)^\beta \right], \quad (21)$$

being GP the generalized parameter (i.e., the uniaxial applied stress), B and C two asymptotic values, and β and δ two constant coefficients. Given the cdfs of the fatigue life associated with the two failure modes, the cdf of the fatigue life is obtained by applying the weakest link principle:

$$F(N_f; GP) = 1 - \prod_{i=1}^2 (1 - F_i(N_f; GP)). \quad (22)$$

The methodology has been validated on a literature dataset⁶⁵ for which the experimental failures originated from the specimen surface in the LCF-HCF region and from internal defects in the VHCF region. Figure 17A shows the P-S-N curves obtained by considering the two failure modes separately, whereas Figure 17B shows the “combined P-S-N curves” at different failure probabilities. The estimated P-S-N curves are compared with those estimated in Paolino et al.⁶⁶ The model is in

agreement with the experimental data: Differently from Paolino et al.,⁶⁶ a clear transition between the two failure modes is not present, and the S–N curves seem to show a continuous decreasing trend in the VHCF region, without an asymptotic trend indicating the occurrence of a fatigue limit for the second failure mode. Considerations on the existence of the fatigue limit and on its proper estimation were made by the same research group in Fernández-Canteli et al.⁶⁷

In Paolino et al.,⁴⁵ a similar approach has been followed, and a unified statistical model for the P–S–N curves in the LCF–VHCF life range is defined, by modeling also the presence of a VHCF limit. The proposed general model permits assessing the duplex P–S–N curves with different failure modes and with a VHCF fatigue limit (i.e., a horizontal asymptote at the end of the curve associated to the internal failure mode in VHCF). The cdf of the fatigue life F_Y (Y is the rv representing the fatigue life) is given by

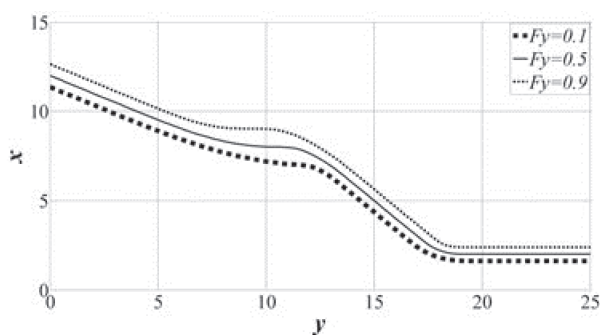
$$F_Y = F_{Y|surf} \cdot F_{X_t} + (1 - F_{X_t}) F_{Y|int} \cdot F_{X_l}, \quad (23)$$

being $F_{Y|surf}$, $F_{Y|int}$ the cdfs of the fatigue life associated to the surface and to the internal failure modes, F_{X_t} the cdf of the transition stress, and F_{X_l} the cdf of the fatigue limit. $F_{Y|surf}$ and $F_{Y|int}$ are assumed to be normally distributed. The mean values of $F_{Y|surf}$ and $F_{Y|int}$ are assumed to be a linear function of the logarithm of s_a . The standard deviation of $F_{Y|surf}$ and $F_{Y|int}$ is assumed to be constant or linearly dependent on the logarithm of s_a . F_{X_t} and F_{X_l} are assumed to be log-normally distributed. The proposed model has been validated on literature datasets. Figure 18A shows the simulated 0.1th, 0.5th, and 0.9th quantiles of the duplex P–S–N curves estimated with the model in Equation 23. The proposed cdf for the fatigue life in the LCF–VHCF life range has been further

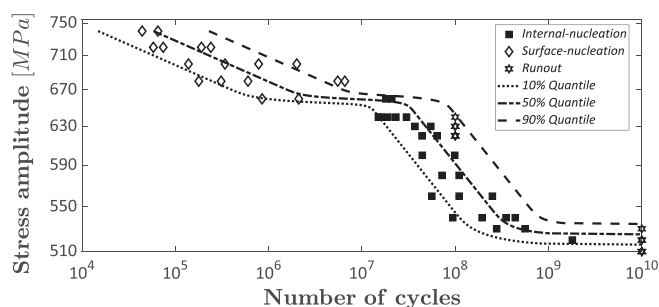
validated in Paolino et al.⁶⁸. In particular, a procedure for the estimation of the unknown parameters and for the probabilistic prediction of the failure mode of each tested specimen is proposed. The 0.1th, 0.5th, and 0.9th quantiles of the P–S–N curves estimated by considering a literature dataset are shown in Figure 18B, showing a good agreement with the experimental data.

The model for the fatigue life in the VHCF region in Equation 23 has been further developed by the same research group in Paolino et al.^{36,37} (Section 3.3.1, Equation 17), in order to model the influence of defect size on the crack nucleation process in VHCF. Equation 17 can be inserted in Equation 23 (i.e., $F_{Y|int} \cdot F_{X_l} = F_{Y|int}(y;x)$) to take into account the influence of defect size in VHCF and to obtain an even more general formulation.

In Sun et al.,⁶⁹ differently from the above-described models, the fatigue life is assumed to continuously decrease with the applied stress amplitude even in the VHCF region, with the same trend found for HCF data and regardless of the failure mode. Therefore, a knee point or a transition stress has not been modeled, and a unique Basquin model is assumed for modeling the fatigue life. Moreover, the statistical distribution of the $\log_{10}(N_f)$ is analyzed for different literature datasets, showing that both a Weibull distribution and a normal distribution can be used to model the fatigue life in VHCF. By analyzing the P–S–N curves, with material parameters estimated through the application of the maximum likelihood principle, the authors show that a continuous decreasing trend is appropriate for modeling the fatigue life, since all the experimental data are above the 95th quantile S–N curve, with the Weibull cdf for the fatigue life being more conservative. Thereafter, this model is exploited to model the influence of the specimen size on the VHCF response. Large specimens (or large components) are assumed to be composed by n small



(A)



(B)

FIGURE 18 Validation of the model for the VHCF life in Paolino et al.^{45,68}: (A) simulated 0.1th, 0.5th, and 0.9th quantiles of the duplex P–S–N curves estimated with the model in Equation 23 (Paolino et al.⁴⁵) (reprinted with permission from Wiley) and (B) duplex P–S–N curves estimated by considering a literature experimental dataset in Paolino et al.⁶⁸ (experimental data digitized from the original figure)

specimens, and a weakest link approach is applied, with the fatigue life for large specimens (or components) being the minimum among the fatigue life of n small specimens. The model has been validated on an experimental dataset on high-strength steels.⁷⁰ Figure 19 shows the estimated P-S-N curves (Figure 19A for the specimens “SUP Heat B” in Furuya⁷⁰ and Figure 19B for the specimens “SUP Heat C” in Furuya⁷⁰), proving the effectiveness of the model, since both the experimental failure for small specimens ($V_{90}=33\text{ mm}^3$) and large specimens ($V_{90}=912\text{ mm}^3$) are above the estimated 99.9% P-S-N curve.

Apetre et al.⁷¹ and Arcari et al.⁷² focused on the strain–life relation, by exploiting the properties of the Weibull distribution. A probabilistic model for the assessment of the strain–life curves capable to fit experimental data obtained through CA tests and to model the influence of the stress ratio on the VHCF response has been proposed. Starting from the probabilistic strain–life Weibull regression model in previous studies,^{73–76} a general formulation for the relation between the strain amplitude ε_a and N_f is defined:

$$\varepsilon_a \cdot \left(\frac{2}{1-R}\right)^{1-\hat{\gamma}} = \exp\left(\alpha_1 + \frac{\lambda + \delta \cdot [(-\log(1-p))]^{1/\beta}}{\log N_f - \alpha_2}\right), \quad (24)$$

being R the stress ratio; $\hat{\gamma}$ a parameter that accounts for the stress ratio sensitivity; α_1 , α_2 , λ , δ , and β constant coefficients that must be estimated from the experimental data; and p the probability of failure. The procedure for the parameter estimation is also provided in the paper,

involving a constrained least-square method. The model has been validated on literature datasets obtained by testing 7075-T6 specimens. Figure 20 plots the Walker strain amplitude, $\varepsilon_a \cdot \left(\frac{2}{1-R}\right)^{1-\hat{\gamma}}$, with respect to N_f . According to Arcari et al.,⁷² the Walker method has shown to be effective in modeling the mean stress effect. The authors conclude that the model is in good agreement with the experimental data and that it has a better fitting capability in the VHCF region than the “conventional fit” (black line). With conventional fit, Arcari et al.⁷² refer to a conventional strain–life fit by using linear regression. Accordingly, the strain life behavior and the corresponding probability of failure can be properly assessed with the proposed model, regardless of the failure mode.

In the paper, VA fatigue tests were also carried out. The proposed formulation can be effectively used for considering the influence of the stress ratio and of the mean stress, but not for VA loading, since the statistical distribution of the VA loading is not modeled. VA tests have been carried out to show that small amplitude loads can have a significant influence on the fatigue life. The results of the VA fatigue tests have been analyzed with the model in Arcari et al.⁷² by using the rainflow counting method to identify the fatigue cycles in the spectrum and the Miner’s rule to sum the damage produced by each cycle in the spectrum block. However, the proposed model cannot account for the shape of the cumulative loading spectrum.

The model in Liu et al.⁷⁷ is also worth to be mentioned, even if the P-S-N curves are finally not estimated. In Liu et al.,⁷⁷ the probability associated with three failure modes (“surface without facets,” “surface with

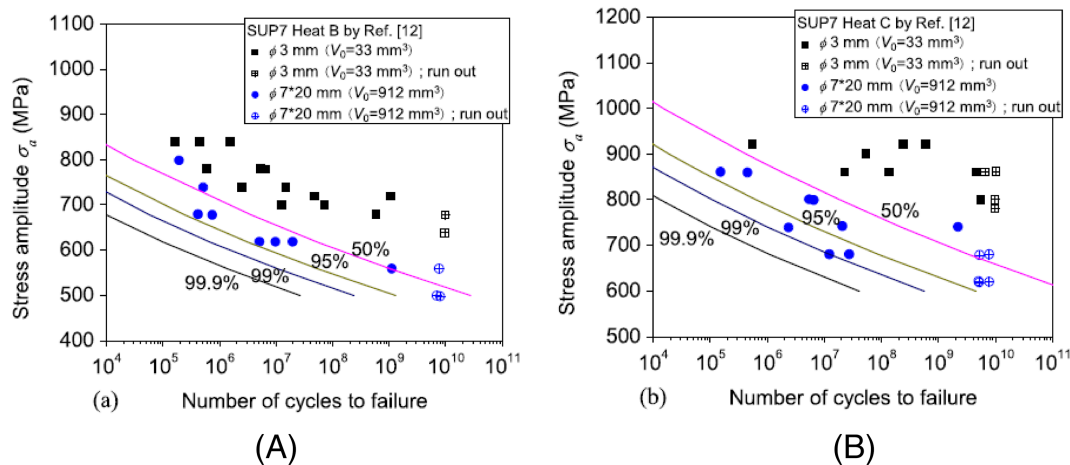


FIGURE 19 Validation of the model for the VHCF life in Sun et al.⁶⁹: (A) P-S-N curves estimated by considering the specimens “SUP Heat B” in Furuya et al.⁷⁰ and (B) P-S-N curves estimated by considering the specimens “SUP Heat C” in Furuya⁷⁰ (reprinted with permission from Elsevier) [Colour figure can be viewed at wileyonlinelibrary.com]

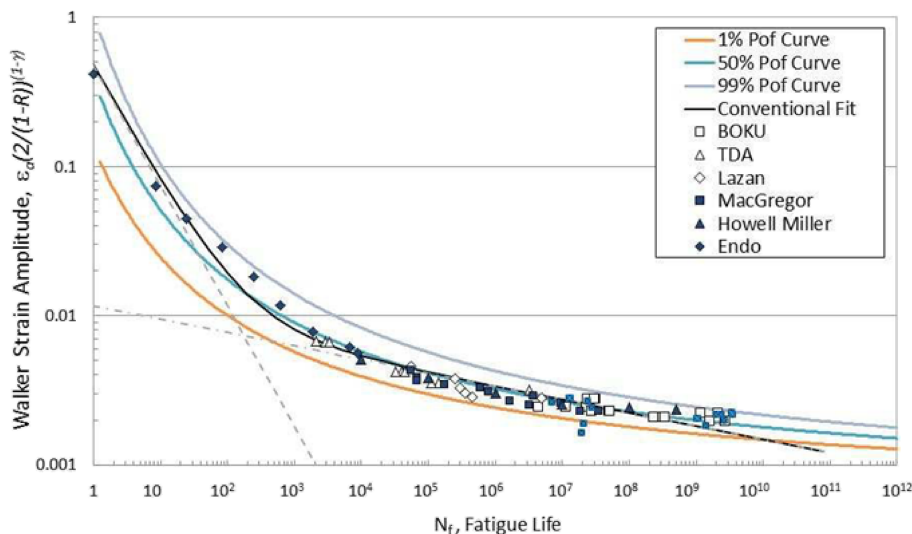


FIGURE 20 Validation of the model for the VHCF life in Arcari et al.⁷²: Walker strain parameter with respect to N_f (reprinted with permission from Elsevier) [Colour figure can be viewed at wileyonlinelibrary.com]

facets,” and “interior with facets”) for a Ti6Al4V alloy is estimated. The normal distribution is considered for computing the probability of a cleavage failure for a grain. The probability of a defect from which the crack could propagate, on the other hand, is assessed through a two-dimensional Poisson distribution, which permits assessing the probability of “activated defect” among a number of defects present within the material. By evaluating the total number of critical internal defects and of critical surface defects that may cleavage, the probabilities of a surface failure with facets, of an interior failure with facets and of a surface failure without facets, are finally computed. The probabilities associated to these three types of investigated failures are finally plotted against the maximum stress, but no indication on how to assess the fatigue life and to estimate the P-S-N curves is proposed.

All the models analyzed in this section have proved that either Weibull distribution or a normal distribution can be exploited for the assessment of the fatigue life even in the VHCF region. Moreover, they focus on the importance of properly accounting the possible presence of two failure modes, with a transition stress or a knee point. The occurrence of two failure modes, moreover, involves the presence of a larger number of parameters that have to be estimated from the experimental data. The procedure for parameter estimation can be rather complex, and optimization algorithms should be employed. For example, for the application of the maximum likelihood principle,⁴⁵ optimization algorithms have to be used (e.g., the simplex search method implemented in Matlab). These algorithms require an initial guess of the parameters to be optimized that have to be properly chosen in order to obtain a physical solution and to avoid obtaining a local maximum of the function

to be maximized. This complexity could discourage their use for practical applications. However, if the procedure for parameter estimation is automated, the use of these methodologies based on the assumption of the statistical distribution of the fatigue life can be further extended. Indeed, according to the above analyses, they have proved to be effective in modeling the P-S-N curves in both the VHCF life range and the LCF-VHCF life range. It is worth noting that, as the number of parameters involved in the models increases, the computation time increases: However, with the proper programming strategy, computation time can be limited and reasonable (minutes). Moreover, all the model involved a transition stress or a knee point, apart the model in Sun et al.⁶⁹: The possible presence of a transition stress must be verified case by case, depending on the tested material and on the experimental datasets. However, the assumption of a specific trend for the entire LCF-VHCF life range (i.e., a linear decreasing trend) is not suggested or has to be avoided: Indeed, the models must be general (i.e., admitting the presence of multiple failure modes) and capable to properly adapt to the shape and the trend of the experimental data. Therefore, the model in Sun et al.⁶⁹ is valid only for specific datasets showing linear decreasing trend, whereas the other analyzed models are more general and, with the proper parameter estimation strategy, have the capability to adapt to different datasets. The models analyzed in this section have been validated mainly on high-strength steels, and their validity must be proved on datasets obtained by testing different materials. It must be also noted that, if defects are at the origin of the fatigue failures, their influence cannot be neglected and should be modeled. Therefore, more efforts should be made to model the dependence of the fatigue on the defect size. The influence of the mean stress, or the stress

ratio, is not considered in the analyzed models, apart from in Arcari et al.⁷² This shortcoming must, necessarily, be addressed in future research to extend the range of application of models based on a probabilistic approach.

3.4 | Models for the S–N curves: Fracture mechanics approach

In this section, models for the fatigue life based on the fracture mechanics approach are analyzed. It is worth noting that models based on the integration of the Paris law can be included within this macro category. However, a classification that distinguishes between “fracture mechanics” approach and models based on the “integration of the Paris laws” would help the reader, according to our opinion.

In order to apply a fracture mechanics approach, the dependence between the fatigue life and the defect size is implicit (i.e., this approach must necessarily consider the presence of a defect or of a crack), differently from the models based on a probabilistic approach for which this dependence is not required and must be a priori assumed. In general, within this group, models that involve the estimation of the SIF or of the SIF threshold are considered. On the other hand, the statistical scatter is generally neglected, even if it is fundamental when dealing with the fatigue response.

In Chapetti et al.,^{33,34} a combined experimental–fracture mechanics approach is proposed. In particular, the dependency between $\sqrt{a_{d,0}}$, the FGA size, $\sqrt{a_{FGA}}$, and N_f , obtained by interpolating experimental VHCF literature data on quenched and tempered steels (JIS SUJ2, SCM435, and SNCM439 steels):

$$\frac{\sqrt{a_{FGA}}}{\sqrt{a_{d,0}}} = 0.25 \cdot N_f^{0.125}, \quad (25)$$

Equation 25 interestingly shows that, given $\sqrt{a_{d,0}}$, N_f increases with FGA size. However, it is worth noting that the constant coefficients (i.e., 0.25 and 0.125) involved in the equation may vary depending on the material type and on delivery condition. According to this dependence, the authors, moreover, assume that the number of cycles consumed to create the FGA is representative of the total fatigue life and that the threshold stress range $\Delta\sigma_{th}$, obtained by equating the SIF threshold and the SIF associated with the initial defect, can be expressed as

$$\Delta\sigma_{th} \cdot a^{\frac{1}{6}} = 3.55 \cdot (HV + 120), \quad (26)$$

being a the crack length. By substituting Equation 25 in Equation 26, the fatigue life as a function of the stress amplitude and the defect size is obtained:

$$\Delta\sigma_{th} \cdot N_f^{\frac{1}{48}} = 4.473 \cdot \frac{(HV + 120)}{R_i^{1/6}}, \quad (27)$$

being R_i the inclusion radius. It must be noted that the internal fatigue limit in Equation 2 has been obtained from Equation 26 and by considering a crack that is three times larger than the largest inclusion, in order to model the weakening mechanisms inducing the FGA formation. On the other hand, the dependency between the applied stress, the characteristic defect size and N_f in Equation 27 has been obtained by inserting Equation 25 in Equation 26. The model is validated on literature datasets. Figure 21 shows the literature datasets ([5] in the figure is Shiozawa and Lu⁴³ in the present paper, and [23] in the figure is Chen et al.⁷⁸ in the present paper) and the estimated S–N curves (the line associated with Equation 27 in the figure indicated by the red arrow).

According to the authors, the slope of the curve estimated by considering an inclusion radius $2 \cdot R_i^{max} = 22 \mu\text{m}$ (i.e., two times the largest inclusion found in the literature for the same material) is in agreement with the experimental data. The distribution of the fatigue life is

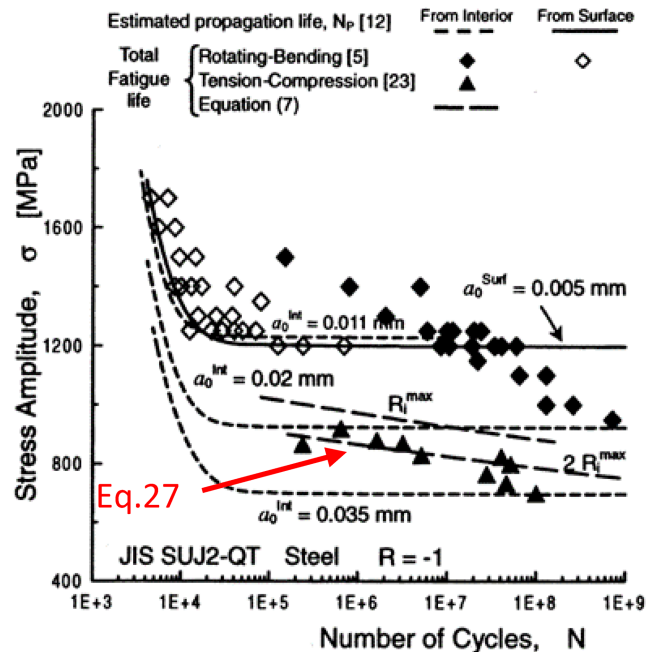


FIGURE 21 Validation of the model for the VHCF life in Chapetti et al.³⁴: experimental data and estimated model on an S–N plot (reprinted with permission from Elsevier) [Colour figure can be viewed at wileyonlinelibrary.com]

not investigated, and a procedure for the estimation of the curves at different failure probabilities is not provided in the paper.

In Bandara et al.,²⁵ the relation between the fatigue life, the applied stress, the defect size, and the stress ratio is obtained starting from the Murakami formulation and the models in Wang et al.^{79,80} The following equation is valid for internal failures:

$$s_{a,int} = (3.09 - 0.120 \cdot \log_{10} N_f) \cdot \frac{(HV + 120)}{(\sqrt{a_{d,0}})^{1/6}} \cdot \left(\frac{1-R}{2}\right)^\alpha, \quad (28)$$

whereas Equation 29 is valid for surface failures:

$$s_{a,surf} = (2.79 - 0.108 \cdot \log_{10} N_f) \cdot \frac{(HV + 120)}{(\sqrt{a_{d,0}})^{1/6}} \cdot \left(\frac{1-R}{2}\right)^\alpha. \quad (29)$$

Moreover, a formulation for eliminating the dependence on $\sqrt{a_{d,0}}$, which may be difficult to be estimated, is proposed:

$$s_a = (155 - 7 \cdot \log_{10} N_f) \cdot \frac{(HV + 120)}{1000} \cdot (R_u)^{1/3} \left(\frac{1-R}{2}\right)^\alpha, \quad (30)$$

being R_u the ultimate tensile strength. The numeric constants in the formulation (155, 7, 2.79,) have been obtained by analyzing literature results on high-strength

steels. The model has been validated by considering 58 experimental fatigue strengths of high- and medium-strength steels obtained through rotating bending and ultrasonic axial fatigue tests. Figure 22 compares the predicted fatigue strength (σ'_w) with respect to the experimental fatigue strength σ_w for $R = -1$ and for $R = 0$ computed with Equation 30. The data obtained with the model in Equation 30 are those indicated with *Bandara et al. Equation (17)* in Figure 20A, whereas they are those indicated with *Equation 17* in Figure 20B. According to Figure 20A, the model is in agreement with the experimental data, with the datapoints close to the bisector. However, about the half of the data is below the bisector, being the prediction nonconservative. Figure 20A,B confirms moreover that the model is capable to assess the influence of the stress ratio. Other validations are moreover carried out in the paper. The approach proposed in this paper is interesting, since it permits to account for the influence of the defect size and the stress ratio and proposes an alternative solution for the estimation of the largest defect based on the tensile strength. However, a procedure for the assessment of the quantiles of the curves is not provided. Moreover, the numeric constants in the formula are estimated under reasonable assumptions and by considering a quite large number of experimental data on steel: However, further validations are required to prove that the models in Equations 29 and 30 can be generally used for steels. A procedure for the estimation of the quantiles of the curves is fundamental, if the model has to be applied for the design of components without an experimental estimation and validation of the material constant parameters.

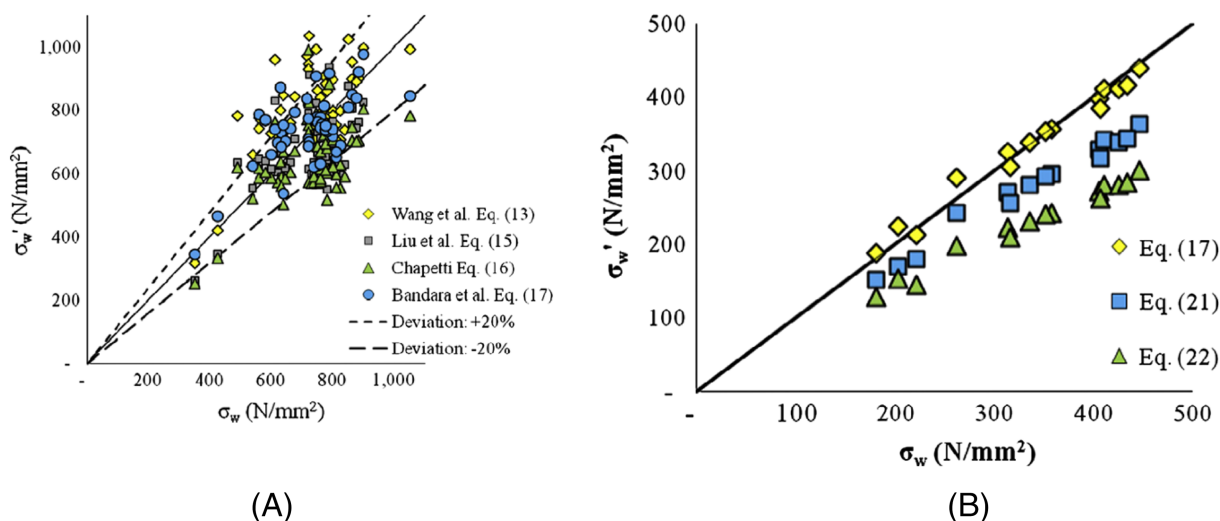


FIGURE 22 Validation of the model for the VHCF life in Bandara et al.²⁵: predicted fatigue strength (σ'_w) with respect to the experimental fatigue strength σ_w . (A) $R = -1$ and (B) $R = 0$ (reprinted with permission from Elsevier) [Colour figure can be viewed at wileyonlinelibrary.com]

In Kolyshkin et al.,⁸¹ a VHCF life model based on the inclusion distribution within the material volume and on a fracture mechanics approach is proposed and validated on a dataset obtained by testing an AISI 304 steel. This approach involves an experimental–analytical approach, and it permits estimating the P–S–N curves at different failure probabilities. By assuming that VHCF failures originate from very large inclusions within the material, only the inclusions exceeding a threshold size are to be considered and are assumed to follow a generalized Pareto distribution function. For the investigated steel, the threshold was assumed to be 12 μm , whereas the other material parameters involved in the Pareto distribution function are estimated from the experimental data. The distribution of the inclusions above the threshold in the normal direction (ND, i.e., along the thickness) is, on the other hand, assumed to follow a Cauchy cdf. By reasonably assuming that the interaction among inclusions is negligible, a procedure based on the Monte Carlo simulation is proposed and applied to the experimental dataset. Each simulation involves the following steps:

1. Generation of the inclusion population within the investigated risk volume V_{95} (i.e., the specimen volume characterized by a stress amplitude larger than the 95% of the maximum applied stress). A Woodhead analysis is applied to assess the density of inclusions, whereas the size and the location of the inclusions above the selected threshold size within the investigated risk volume are modeled according to the Pareto and the Cauchy distributions, respectively. The stress in the vicinity of each inclusion is obtained analytically. It is worth noting that the parameters of the Pareto and the Cauchy distributions must be estimated from the experimental results, for example by analyzing the fracture surfaces of specimens subjected to VHCF tests.
2. Depending on the inclusion location, computation of the shape factor Y involved in the SIF equation.
3. Computation of the SIF associated to each inclusion.
4. Calculation of the fatigue life, N_f , by assuming that the crack initiates simultaneously at all the considered inclusions. N_f is obtained from the curve SIF versus N_f , estimated by fitting experimental results already obtained for the tested material.
5. Identification of the inclusion characterized by the smallest N_f , the one that will originate the fatigue failure.

The procedure is repeated iteratively, at least 100 times, for the stress amplitudes that are supposed to be applied experimentally. The simulated sizes and locations are found to be in agreement with those found

experimentally. In order to take into account the scatter associated with the defect size and location, the quantiles of the P–S–N curves for the tested steel are estimated from the 100 simulations. In particular, the estimated fatigue lives (i.e., one estimated fatigue life in each simulation) are ordered in ascending order for each considered stress level, and the values of the 10%, 50%, and 90% percentiles are considered for the estimation of the P–S–N curves at the corresponding failure probability, as shown in the S–N plot in Figure 23 (in our opinion, the solid line curves correspond to the 0.1th and the 0.9th quantiles curves, even if they are indicated with “10% confidence” and “90% confidence” in the legend). According to Figure 23, all the data are within the estimated 10% and 90% P–S–N curves; moreover, Figure 23 shows that the scatter is larger at higher stress amplitudes, where two damage mechanisms are present, whereas it reduces as the applied stress amplitude decreases, in the fatigue life range where only internal failures are present.

According to these analyses, a pure fracture mechanics approach has been employed in three literature papers. Indeed, the approaches based on the analysis of the SIF or, more specifically, of the SIF threshold are more appropriate for the assessment of the fatigue limit, as pointed in Section 2. Nevertheless, the model analyzed in this section proved to be effective and in agreement with the literature data. The model in Chapetti et al.³⁴ can be easily applied and permits taking into account the influence of the FGA formation in the crack nucleation process. However, it involves the estimation of the SIF threshold, which may vary depending on the material, heat treatment, and production process and cannot be easily retrieved or experimentally estimated. The constant material parameters in Equation 25 should be

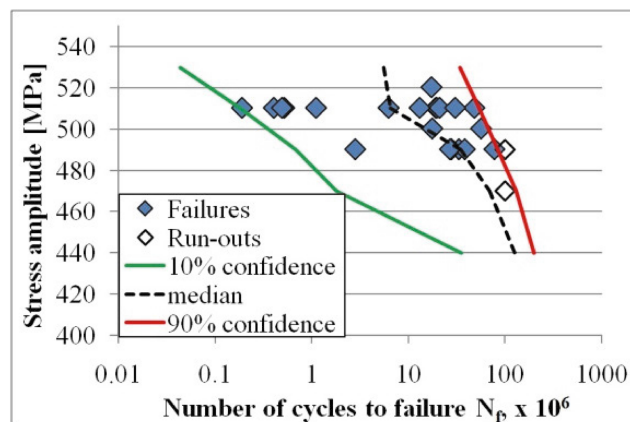


FIGURE 23 Validation of the model for the VHCF life in Kolyshkin et al.⁸¹: experimental data on the S–N plot and estimated P–S–N curves (reprinted with permission from Elsevier) [Colour figure can be viewed at wileyonlinelibrary.com]

verified for each investigated material. Moreover, no details on the statistical distribution of the fatigue life are provided, in order to take into account the experimental data scatter. In Bandara et al.,²⁵ an interesting approach is proposed to model the relation between the fatigue life, the applied stress, the defect size, and the stress ratio. The defect size is estimated by considering the material tensile strength. Indeed, the expected defect in the material volume may be hard to estimate or predict if the distribution of defect size is not available. A procedure for the assessment of the quantiles of the curves or to take into account the scatter associated to the fatigue response is not provided.

In the model in Kolyshkin et al.,⁸¹ the dependence between the SIF associated to the defect and the number of cycles to failures has to be estimated from the experimental data. The distribution of inclusion size and inclusion location is also considered, and they have to be both experimentally assessed. By applying an iterative procedure, the quantiles of the P-S-N curves are reliably assessed.

These three methodologies showed how an approach based on the SIF or on the SIF threshold can be effective for modeling the fatigue life in VHCF. This approach, however, requires necessarily a fundamental analysis of the experimental results and of the fracture surfaces in order to define the coefficients involved in the equations that link $\frac{\sqrt{a_{ODA}}}{\sqrt{a_{d,0}}}$ with N_f (Chapetti et al.³⁴) or the SIF associated to defects to N_f (Kolyshkin et al.⁸¹) that are generally not required in models based on a probabilistic approach. Or, at least, if the models are intended to be valid for a wide range of steels (Bandara et al.,²⁵), the sensitivity of the material parameters in the SIF threshold equation or in the SIF equations should be verified. On the other hand, the term $\sqrt{a_{d,0}}$ is replaced by considering the material tensile strength in Bandara et al.,²⁵ but this assumption must be verified on a large number of datasets to be accepted for all steels.

3.5 | Models for the S-N curves: Integration of the Paris law

In this section, the models based on the integration of the Paris law are analyzed and described. Through this approach, the dependence between N_f , s_a , and the defect size can be assessed. In particular, the crack propagation from the defect to the FGA, generally neglected with the approaches described above, is modeled.

In Tanaka and Akiniwa,⁴⁷ the stress-life relation is obtained by analyzing the crack formation and propagation from the initial defect. Two S-N curves, one for

cracks originating from surface defects and one for cracks originating from internal defects, are estimated by integrating the Paris law. The models are validated on experimental results obtained by testing the bearing steels JIS, SUJ2 and a low-alloy steel, JIS SNCM439. The crack propagation from internal defects takes place in two stages: Stage 1, from the inclusion to the border of the FGA, and Stage 2, with crack propagation as a “long crack.” The crack propagation in Stage 1 and Stage 2 can be modeled with the Paris law. The SIF threshold range for internal cracks, $\Delta k_{th,i}$, is assumed to be constant. Stage 1 and Stage 2 occur for internal cracks, whereas Stage 1 is not present for surface cracks. Accordingly, two S-N curves are estimated: the S-N curve for surface crack nucleation and the S-N curve associated to the internal failure mode. The conventional fatigue limit is denoted as the fatigue limit for the surface failure mode. The constant coefficients are computed by minimizing the differences between the experimental N_f and the estimated N_f , assessed through the integration of the Paris law.

Figure 24 plots the experimental data and the estimated S-N curves in an S-N plot.⁴⁷ The estimated S-N curves have been found to be in good agreement with the experimental data. It was moreover shown that the S-N curves estimated with the proposed model can be used to compute the influence of specimen diameter, loading mode, and residual stress. The statistical distribution of the fatigue life is not discussed, and the P-S-N curves at different failure probabilities are not estimated in the paper.

In Lu et al.,⁸² three failure modes are found by testing a high-chromium bearing steel, GCr15, in the LCF-VHCF life range: surface-induced fracture mode, S mode;

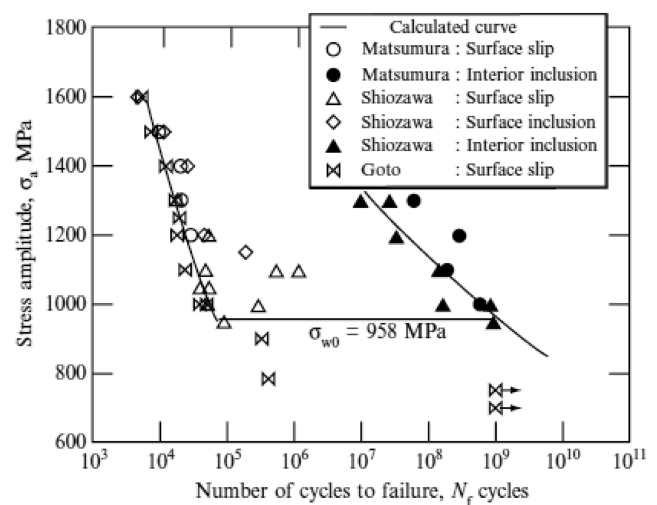


FIGURE 24 Validation of the model for the VHCF life in Tanaka and Akiniwa⁴⁷: experimental data and estimated model on an S-N plot (reprinted with permission from Wiley)

internal inclusion-induced fracture mode without a formation of the FGA area, I mode; internal inclusion-induced fracture mode with the FGA area formation, IG mode. The work is moreover focused on the influence of the defect size on the fatigue life, by assuming that the fatigue crack propagation from the initial defect to the FGA can be described by the Paris law. N_f is therefore obtained through the integration of the Paris law, under the reasonable assumption that N_f is mainly consumed to form the FGA and that the crack propagation outside the FGA can be neglected:

$$N_f = \frac{\left(1 - (\sqrt{a_{d,0}}/\sqrt{a_{FGA}})^{(m/2-1)}\right)}{C \cdot (0.5 \cdot s_a \cdot \sqrt{\pi})^m \cdot (m/2-1)} \cdot \frac{1}{(\sqrt{a_{d,0}})^{(m/2-1)},} \quad (31)$$

being m , C constant coefficients and $\sqrt{a_{d,0}}$ and $\sqrt{a_{FGA}}$ the square root of the area of the initial defect and of the GBF, respectively. It was assumed that $\sqrt{a_{d,0}}/\sqrt{a_{FGA}} \cong 1.18$ and that m is significantly larger than the values assumed for a propagation outside the FGA (e.g., larger than 7), so that $(\sqrt{a_{d,0}}/\sqrt{a_{FGA}})^{(m/2-1)}$ can be neglected. According to these further assumptions, Equation 31 can be rewritten as Equation 32, which expresses the relation between the fatigue life N_f and the applied stress s_a in the presence of an initial defect with size equal to $\sqrt{a_{d,0}}$:

$$\left(0.5 \cdot s_a \cdot \sqrt{\pi \sqrt{a_{d,0}}}\right)^m \cdot \frac{N_f}{\sqrt{a_{d,0}}} = \frac{2}{C \cdot (m-2)}. \quad (32)$$

The unknown parameters m , C are estimated from the experimental data and by applying the least-square method. By replacing the constant coefficients 0.5 with 0.65 and $\sqrt{a_{d,0}}$ with $\sqrt{A_S}$ (size of a surface defect), Equation 32 can be used to compute the relation between the fatigue life and the applied stress for a surface defect. The model has been validated on the dataset obtained by the authors, by considering $\sqrt{a_{d,0}}$ equal to 16 μm (average internal inclusion size for the IG mode) and to 20 μm (size of an inclusion in axial loading) and $\sqrt{A_S}$ equal to 9 μm . Figure 25 shows the experimental data and the S–N curves estimated with Equation 32. According to the authors, the curve for IG mode and $\sqrt{a_{d,0}} = 16 \mu\text{m}$ is in agreement with the experimental failures. For the other failure modes, there are not enough experimental data to validate the model. The distribution of the fatigue life is not defined in the paper. In the figure, $\sqrt{A_{IG}}$ corresponds to $\sqrt{a_{d,0}}$.

It must be noted that the failure modes considered in this paper (Lu et al.⁸²) are the same as investigated in Li et al.⁶¹ Differently from the other models, in Li et al.⁶¹ and Lu et al.,⁸² the authors distinguished between

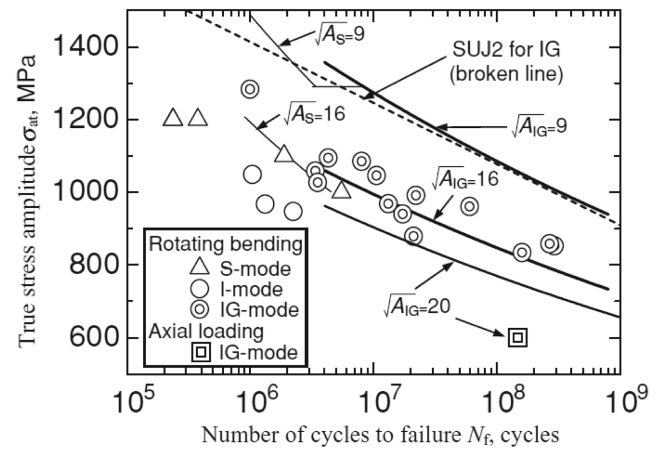


FIGURE 25 Validation of the model for the VHCF life in Lu et al.⁸² (reprinted with permission from Wiley)

failures from defects without FGA formation and failures from defects with FGA formation. Accordingly, they assume that the experimental data follow two different trends in an S–N plot (Figures 16A and 25), depending on the FGA formation around the defects. For the other investigated datasets that show surface failures in the LCF–HCF life range and internal failures from defects in the VHCF life range, different trends, depending on the FGA formation, were not observed and, therefore, not modeled.

In Schuller et al.,⁸³ differently from Mayer et al.⁴⁸ where the same research group modeled the stress life relation by combining the Basquin equation and the Murakami formulation, the final relation between N_f , s_a , and $\sqrt{a_{d,0}}$ is obtained by integrating an adapted Paris law:

$$N_f = \frac{2}{C \cdot (n-2) \cdot (\sqrt{\pi})^n} \cdot (s_a)^{-n} \cdot \sqrt{a_{d,0}} \cdot \left(\frac{2-n}{2}\right). \quad (34)$$

The experimental data, obtained through ultrasonic tension–compression tests on 18Ni maraging steel thin sheets with different Co and Ti content and the estimated models, are shown in the modified S–N plot in Figure 26. The authors proposed also to assess the scatter associated with the experimental data by assuming a log-normal distribution for the fatigue life, but in the figure only the median curves are shown. With this approach, on the other hand, the influence of the FGA on the crack nucleation is not taken into account. Material A and Material B are the same material, but Material B has a larger content of Co, which increases the strength. Moreover, Ti is eliminated in Material B.

In Paolino et al.,³⁷ the model proposed by the research group of the Politecnico di Torino in the

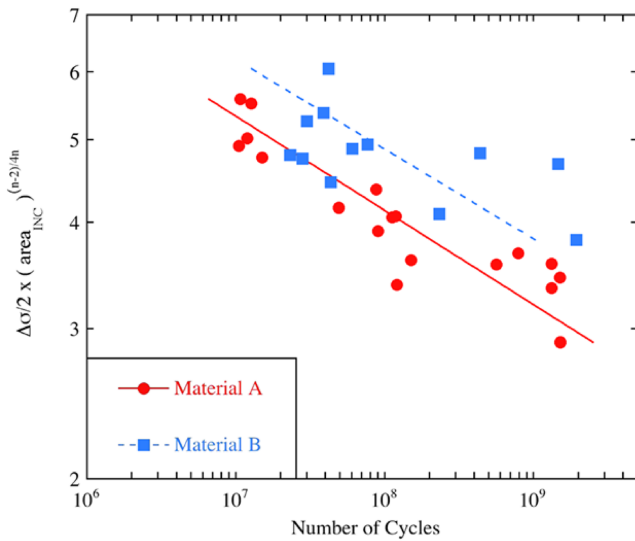


FIGURE 26 Validation of the model for the VHCF life in Schuller et al.⁸³: S–N plot with normalized stress amplitude (reprinted with permission from Wiley) [Colour figure can be viewed at wileyonlinelibrary.com]

previous study³⁶ has been further generalized in a statistical framework, and the unknown parameters are estimated by integrating the Paris law that models each stage of crack growth from the internal defect up to the final failure. In particular, the α_{th} quantile of the fatigue life is obtained by integrating the Paris law in Stage 1 (from the defect size to the border of the FGA size) and by assuming that the total number of cycles to failures can be approximated by the number of cycles consumed in Stage 1 (i.e., the same assumptions of the model in Lu et al.⁸²):

$$n_{f,\sqrt{a_{d,0}},\alpha_{th}} \cong n_{I,\sqrt{a_{d,0}},\alpha_{th}} = \int_{\sqrt{a_{d,0}}}^{\sqrt{a_{FGA,\alpha_{th}}}} \frac{da}{c_I \cdot (k_d - k_{th,l,\alpha_{th}})^{m_I}}, \quad (35)$$

being c_I and m_I the constant coefficients involved in the Paris law, $n_{f,\sqrt{a_{d,0}},\alpha_{th}}$ the α_{th} quantile of the total life, $n_{I,\sqrt{a_{d,0}},\alpha_{th}}$ the α_{th} quantile of the number of cycles to failure consumed in Stage 1, k_d the SIF associated to the initial defect size $\sqrt{a_{d,0}}$, $k_{th,l,\alpha_{th}}$ the α_{th} quantile of the local SIF threshold (Section 2), and $\sqrt{a_{FGA,\alpha_{th}}}$ the α_{th} quantile of the FGA size. The α_{th} quantile of the marginal P–S–N curve is given by

$$\alpha_{th} = \int_0^\infty F_{N_f|\sqrt{a_{d,0}}}(n_{f,\alpha_{th}}; s_a, \sqrt{a_{d,0}}) f_{\sqrt{A_{d,0}}}(\sqrt{a_{d,0}}) d\sqrt{a_{d,0}}, \quad (36)$$

being $F_{N_f|\sqrt{a_{d,0}}}(n_{f,\alpha_{th}}; s_a, \sqrt{a_{d,0}})$ the conditional distribution of the fatigue life. $F_{N_f|\sqrt{a_{d,0}}}(n_{f,\alpha_{th}}; s_a, \sqrt{a_{d,0}})$ is implicitly defined in Equation 35, and through a numerical procedure based on the Monte Carlo simulation, the α_{th} quantile of the fatigue life can be obtained from Equation 35. The methodology in Paolino et al.³⁷ is based on fracture mechanics concepts rather than on fitting the experimental data and the distribution of the fatigue life is not a priori assumed.³⁶ However, differently from all the other models for the fatigue life defined in the literature and based on a fracture mechanics approach, the model in Paolino et al.³⁷ permits also computing the S–N curves at different failure probabilities. On the other hand, the procedure for estimating the material parameters is more complex, and a numerical procedure based on the Monte Carlo simulation is necessary. Figure 27 shows the P–S–N curves estimated by considering the experimental dataset obtained by the authors.

In Sun et al.,⁸⁴ the Paris law is not exploited, but the stress life relation is obtained starting from considerations on the crack propagation within the FGA. For this reason, this model has been included in this section. In particular, an equivalent crack length after a number of cycles N is computed by assuming that “the equivalent crack growth rate in the FGA region is related to the maximum size of the plastic zone at the crack tip” and that the number of cycles consumed within the FGA can approximate the total life with negligible differences. The stress–life relation for high-strength steels failing in the VHCF region becomes

$$N_f = \frac{1}{\alpha} \cdot \left(\frac{s_a}{\sigma_Y} \right)^{-l} \ln \left(\frac{a_{FGA}}{a_0} \right), \quad (37)$$

being σ_Y the yield stress, α and l two parameters that have to be estimated from the experimental data, and a_{FGA} the size of the FGA. According to Equation (37), the fatigue life increases with the ratio between the FGA size and the initial inclusion size, in agreement with the experimental evidence. Equation 37, obtained analytically, is similar to that obtained through the interpolation of the experimental data in Chapetti et al.³⁴ and reported in Equation (25). Indeed, they both show that N_f increases with FGA size but with different approaches. Equation 37 with an analytical approach, whereas Equation 25 through an experimental approach.³⁴ The expression obtained by Chapetti et al. depends on two material parameters that have been estimated from the experimental data and that must be verified for other types of materials or delivery conditions (e.g., heat treatments).

FIGURE 27 Validation of the model for the VHCF life in Paolino et al.³⁷: P-S-N curves and experimental data (reprinted with permission from Wiley)

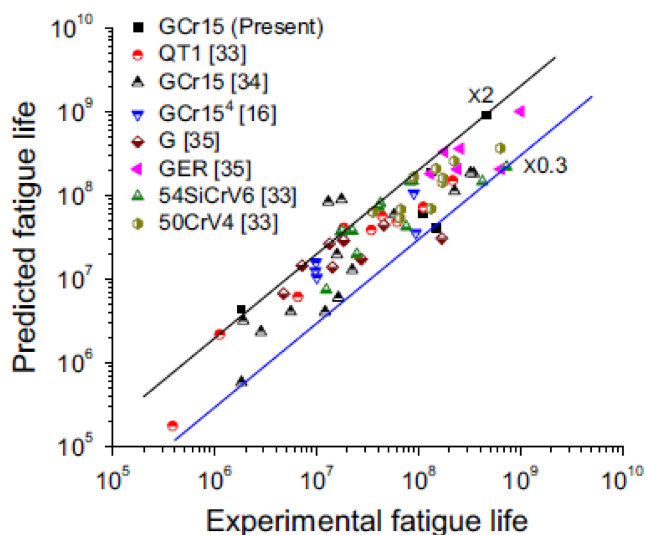
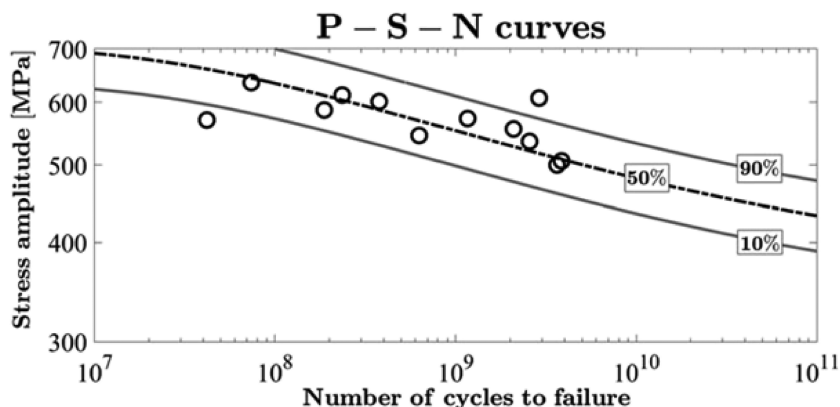


FIGURE 28 Validation of the model for the VHCF life in Sun et al.⁸⁴: predicted fatigue life with respect to the experimental fatigue life (reprinted with permission from Springer) [Colour figure can be viewed at wileyonlinelibrary.com]

The variation of the FGA size with the applied stress amplitude is not accounted in Equation 25. On the other hand, Equation 37 is more general, since it depends on material parameters to be estimated from experimental data, on quasi-static properties, i.e., the yield stress, and on the applied stress amplitude. Accordingly, given the applied stress amplitude, the dependency between the FGA size and N_f can be obtained. The model has been validated on an experimental dataset obtained by testing a high-carbon-chromium steel (GCr15) and on literature datasets. Figure 28 plots the fatigue life predicted with the model in Sun et al.⁸⁴ with respect to the experimental fatigue life. According to Figure 28, the model in Sun et al.⁸⁴ permits to properly predict the fatigue life of specimens failed in the VHCF region with failures showing a fish-eye morphology with FGA formation.

The analysis of the model based on the integration of the Paris law or on the analysis of the number of cycles

consumed within the FGA has shown that also this approach is effective in modeling the stress-life relation. They are almost all based on the assumption that most of the life, larger than 95% to 99%, according to Paolino et al.,³⁷ is consumed within the FGA, according to the experimental evidence. This assumption is generally accepted and has proved to be effective. Moreover, by integrating the Paris law, the dependence between the defect size and the fatigue life is modeled, differently from models for the fatigue life based on a probabilistic approach. The influence of the mechanisms for the FGA formation is, moreover, accounted. However, the material parameters involved in the Paris law equation for the crack propagation within the FGA must be reliably known. The experimental assessment of these coefficients can be rather complex, and, generally, they are not available in the literature. Alternatively, they have to be reliably estimated, even if this could influence the final results. A possible solution can be their estimation through an optimization process: for example, by minimizing the differences between the number of cycles consumed within the FGA experimentally assessed and the estimated number of cycles. This would avoid performing tests for assessing the material parameters in the Paris law equation.

Another critical point of this approach can be the need of measuring the FGA size on the fracture surfaces. Indeed, this requires the availability of a Scanning Electron Microscope (SEM) and a time-consuming analysis of the fracture surfaces.

Another aspect that must be highlighted is that the experimental scatter is generally not modeled with the above-described approach. Indeed, apart from the model in Paolino et al.,³⁷ only the median curve is estimated, and a procedure for the estimation of the quantiles associated to the estimated P-S-N curves is not provided. Therefore, more attention should be paid to this aspect, i.e., modeling also the randomness associated to the fatigue phenomenon or to the defect size, in order to

employ models based on this approach in practical applications.

3.6 | Summary and considerations on fatigue design

In this section, the models described in previous sections are described. Table 1 summarizes the main features associated with each model available in the literature. The models have been subdivided according to the “approach-based” classification followed in the paper. In the first column, the reference number is reported. In the second column, the main features associated to the model are schematically described. In the third, fourth, and fifth columns, the material considered for the validation, the number of investigated failure modes, and the investigated life range are reported, respectively. In Table 1, only the models that focus on the stress–life relation and that propose a procedure for the estimation of the P–S–N curves have been included. The models in previous studies^{44,49,53,77} are not included since they propose interesting approaches for the fatigue life in VHCF, but they have to be further developed for modeling the stress–life relation and, accordingly, the P–S–N curves.

According to Table 1 and to the analyses in the previous section, four main approaches have been followed in the literature:

1. An approach based on the interpolation of the experimental data by exploiting a power law.
2. A probabilistic approach, involving the assumption of the statistical distribution of the fatigue life.
3. A fracture mechanic approach, based on the analysis of the SIF and of the SIF threshold close to the initial defect.
4. An approach based on the integration of the Paris law.

The first approach is the simplest. Indeed, the number of parameters to be estimated is limited, and it is based on the fitting of the experimental data on an S–N plot. However, it fails to account the different mechanisms for crack initiation occurring in VHCF and can be applied only for a specific failure mode. The dependence of the fatigue life on the defect size is generally not considered. On the other hand, in Mayer et al.,⁴⁸ the stress–life relation is assessed by normalizing the stress amplitude by a factor dependent on the defect size. The influence of the stress ratio has been considered in Schönbauer et al.⁵⁰: Starting from the Murakami formulation, the data are normalized by considering the stress ratio. The model in Sun et al.²⁷ is the most general, since

it permits modeling both the influence of inclusion size and the stress ratio and has been validated on experimental datasets obtained by testing high-strength steels. This analysis confirms that a power law is effective in modeling the fatigue life and that, properly adapted, can be exploited also to model the influence of defect size, of the stress ratio or the presence of an asymptote. However, more efforts are necessary to model the scatter associated to the experimental failures and to assess the quantile curves.

The second group includes all the models based on a statistical approach, for which the fatigue response is assessed by fitting the experimental results in an S–N plot and by assuming the distribution of the fatigue life. The fatigue life is assumed to follow a log-normal distribution or a Weibull distribution. These statistical distributions proved to be valid even for the VHCF life range. In particular, the models in Ref.^{6,45,56,57,60–63} focus on the competition between the two failure modes, surface for the LCF–HCF region and internal for the VHCF region. On the other hand, in Sun et al.,⁶⁹ the experimental data are interpolated by considering a continuous decreasing trend from LCF to VHCF, regardless of the failure mode, and a transition between the two failure modes has not been investigated. In Sun et al.,⁶⁹ a weakest link approach has been considered. The transition stress between different failure modes is seen as the fatigue limit for a specific failure mode.⁶¹ In Paolino et al.,³⁶ only the VHCF region is taken into account, and a model for the P–S–N curves below the transition stress is proposed. The influence of the defect size is accounted for by assuming that the mean of the fatigue life distribution is dependent not only on the applied stress but also on the defect size. The duplex P–S–N curves can be obtained by integrating the model in Paolino et al.³⁶ with the unified model in Ref.,⁴⁵ as shown in Tridello and Paolino.⁸⁵ The model in Arcari et al.⁷² focused on the assessment of the strain–life response of materials. All the models within this group have been validated experimentally mainly on a high-strength steel, proving their effectiveness. However, to extend their use, validations on different materials are required. Moreover, the influence of defects is not always taken into account, even if it plays a fundamental role in the VHCF crack initiation. For the models addressing the entire LCF–VHCF life range, the assumption of a linear decreasing trend with only a failure model is to be avoided. Indeed, a large number of experimental datasets show a duplex behavior, with two failure modes, depending on the life range. Therefore, the assumption of a unique trend could limit the use of the model. On the other hand, if more failure modes are modeled and a unique trend is observed from the experimental data, the material parameters to be estimated should adapt to

TABLE 1 Summary of the main models considered for the fatigue life in VHCF

Paper	Main features	Material for the validation	Failure modes addressed	Investigated life range
Power law fitting				
Akiniwa et al. ⁴⁶	Fitting of axial and torsional VHCF test results	Oil-tempered Si–Cr steel, JIS G3561, SWOSC-V	Not specified	VHCF life range
Liu et al. ²⁹	Material parameters estimated from the fatigue limit at 10 ⁶ and 10 ⁹ cycles	Spring steel	Failure from defects	VHCF life range
Sun et al. ²⁷	Influence of defect size and on the stress ratio on the VHCF life	High-carbon–chromium steel	Failure from defects	VHCF life range
Mayer et al. ⁴⁸	Influence of defect size on the VHCF life	Bainitic high-carbon–chromium steel	Failures from defects	VHCF life range
Schönbauer et al. ⁵⁰	Influence of the stress ratio on specimens subjected to constant and variable amplitude loads	17-4PH steel	Not specified	VHCF life range
Probabilistic approach				
Paolino et al. ³⁶	Fatigue life log-normally distributed dependent on $a_{d,0}$ and fatigue limit	H13 tool steel	Failures from defects (also with FGA formation)	VHCF life range
Weixing and Shenjie ⁵⁶	Fatigue life distribution has a double-peaked shape	Aluminum alloy LC4CS	Surface and internal failure modes	LCF–VHCF life range
Zhao et al. ⁵⁷	Fatigue life log-normally distributed and probabilistic concurrent model	LZ50 axle steel	One failure mode (not specified)	LCF–VHCF life range: bilinear trend with transition point
Sakai et al. ⁶	Mixed-mode Weibull distribution; two cdfs for surface and internal failures	High-carbon–chromium steel for the bearing	Surface in the LCF–HCF and internal in the VHCF life range	LCF–VHCF life range: duplex trend
Bomas et al. ⁶⁰	Fatigue life assumed to follow a two-parameter Weibull distribution: failure mechanisms statistically independent	Carburized, quenched and tempered steel SAE 5115	“Non-defect” failures and failures from defects	LCF–VHCF life range: bilinear trend
Li et al. ⁶¹	For each failure mode, fatigue life described by a two-parameter Weibull distribution function	Carburized Cr–Mn–Si steel	Three failure modes, depending on the stress amplitude	LCF–VHCF life range with an asymptote for each failure mode
Li et al. ⁶²	Mixed-mode Weibull distribution, with three parameters Weibull distribution for each failure mode	Bearing steel SUJ2	Surface and internal failures	LCF–VHCF trend: monotonic decreasing trend
Muniz-Calvente et al. ⁶³	Weibull distribution for each failure mode: Castillo–Canteli model	Literature datasets on Ti6Al4V	Surface and internal failures	LCF–VHCF life range: duplex trend

(Continues)

TABLE 1 (Continued)

Paper	Main features	Material for the validation	Failure modes addressed	Investigated life range
Paolino et al. ⁴⁵	Unified statistical model: log-normal distribution for the fatigue life, transition stress and VHCF limit	Literature datasets	Surface and internal failures	LCF–VHCF life range: duplex trend with VHCF limit
Sun et al. ⁶⁹	Weibull or log-normal distribution and Basquin model, assessment of size effect	Literature datasets on high-strength steels	Not defined	Continuous decreasing trend in the LCF–VHCF life range
Apetre et al. ⁷¹ and Arcari et al. ⁷²	Strain–life relation, with the probabilistic strain–life Weibull regression model. Influence of stress ratio R	7075-T6 specimens	Not defined	Continuous decreasing trend in the LCF–VHCF life range
Fracture mechanics approach				
Chapetti et al. ³⁴	Experimental dependence between $\sqrt{a_{d,0}}$, $\sqrt{a_{FGA}}$, and N_f and experimental expression for the SIF threshold	Literature datasets on high-strength steels	Failures from defects	VHCF life range
Bandara et al. ²⁵	Dependence between N_f , $\sqrt{a_{d,0}}$, s_a , and R . $\sqrt{a_{d,0}}$ estimated by considering the tensile strength	Literature datasets on high-strength steels	Failures from surface and defects	VHCF life range
Kolyshkin et al. ⁸¹	Dependence between N_f , $\sqrt{a_{d,0}}$, and s_a by considering also the defect location. P–S–N estimation with an iterative procedure	AISI 304 steel	Failures from defects	VHCF life range
Integration of the Paris law				
Tanaka and Akiniwa ⁴⁷	P–S–N curves for surface and internal cracks. Traditional fatigue limit corresponding to the fatigue limit for surface cracks	Bearing steels JIS, SUJ2 and a low-alloy steel, JIS SNCM439	Failures from surface and from defects	LCF–VHCF life range: duplex trend
Lu et al. ⁸²	Propagation from the initial defect to the FGA border: under reasonable assumption, relation between N_f , s_a , and $\sqrt{a_{d,0}}$ assessed	High-chromium bearing steel, GCr15	Three failure modes: surface, internal with FGA, and internal without FGA	LCF–VHCF life range
Schuller et al. ⁸³	Relation between N_f , s_a , and $\sqrt{a_{d,0}}$ and log-normal distribution for the fatigue life	18Ni maraging steel thin sheets with different Co and Ti content	Failures from defects	VHCF life range

TABLE 1 (Continued)

Paper	Main features	Material for the validation	Failure modes addressed	Investigated life range
Paolino et al. ³⁷	Propagation from the initial defect to the FGA border. Procedure for the quantile of the fatigue life based on Monte Carlo simulation	H13 tool steel	Failures from defects	VHCF life range
Sun et al. ⁸⁴	Crack propagation within the FGA: “the equivalent crack growth rate in the FGA region is related to the maximum size of the plastic zone at the crack tip”	High-carbon–chromium steel (GCr15)	Failures from defects	VHCF life range

follow a single trend, if the parameter estimation is properly carried out. On the other hand, apart from Arcari et al.,⁷² the influence of the mean stress is not modeled with this approach.

Differently from the models belonging to the first group, the number of parameters involved in the cdf of the fatigue life can be high, especially if the LCF–VHCF life range is considered, thus requiring an appropriate number of experimental results for a reliable estimation. The flexibility increases with the number of parameters involved; however, this increases the number of experimental data required and could increase the complexity of the procedure for the parameter estimation. For example, for the application of the maximum likelihood principle,^{36,45} optimization algorithms have to be used (e.g., the *simplex search method* implemented in Matlab). An initial and reasonable guess of the parameters to be estimated is required to obtain a physical solution and to avoid obtaining a local maximum of the function to be maximized. This example shows that, as the number of parameters to be estimated increases, the procedure for their estimation becomes more complex and has also to be properly designed. However, with the proper implementation of the procedure for parameter estimation, the computation time can be limited and kept in a reasonable range (minutes).

Macromechanical models based on the analysis of the SIF and of the SIF threshold associated to the initial defect are included within the third group: For example, in Chapetti et al.,³⁴ the S–N curves are estimated through the analysis of the SIF threshold and by fitting of the experimental data to find the relation between the defect size, the FGA size, and N_f . In Bandara et al.,²⁵ the dependence between s_a , N_f , $\sqrt{a_{d,0}}$, and R is obtained starting from literature models. The dependence on $\sqrt{a_{d,0}}$ has

been interestingly eliminated by considering the material tensile strength. The validation has proved the effectiveness of the proposed methodology for steels. Finally, in Kolyshkin et al.,⁸¹ a model that takes into account the distribution of the most critical defects (defects above a selected threshold) and their distribution within the cross-section is developed, with the fatigue life estimated through a procedure based on the Monte Carlo simulation and by considering the experimental relation between the SIF associated with defects and N_f . In all these models, the proper assessment of the SIF threshold is fundamental to model the crack initiation from the initial defect: In Bandara et al.²⁵ and Chapetti et al.,³⁴ the coefficients involved in the SIF threshold equation are considered constant regardless of the material, since they have been estimated by considering a large number of experimental data on steels. In Kolyshkin et al.,⁸¹ differently from the other literature models, the SIF threshold is not considered, and the experimental relation between the SIF associated with a defect and N_f is exploited for assessing the fatigue life. Within this group, the S–N curves at different failure probabilities are estimated in Kolyshkin et al.,⁸¹ whereas they are not considered in Bandara et al.²⁵ and Chapetti et al.³⁴ In general, all the models for the fatigue life based on a fracture mechanics approach permit modeling the dependency between the fatigue life and the initial defect size, which is fundamental for the analysis of the VHCF response; on the other hand, they may involve the experimental estimation of material coefficients that require specific and time-consuming experimental tests, for example, experimental tests for the estimation of the SIF threshold.

With reference to the fourth group, N_f is obtained through the integration of the Paris law from the initial defect size to the FGA size,^{37,47,82,84} by assuming that the

total fatigue life N_f can be approximated with the life consumed in the formation of the FGA. The validation on the experimental datasets has proved the effectiveness of these models and of this assumption. All the models focus on the assessment of the stress–life relation and provide indications for the assessment of the median curve, without providing a detailed procedure for the assessment of the quantile curves, apart from Paolino et al.³⁷ This shortcoming has to be necessarily addressed in future research. However, the main issue associated with this approach could be the proper choice of the material coefficients involved in the Paris law equation, which are generally not available since they have to be estimated through specific complex experimental tests. Therefore, they should be reasonably retrieved from literature data on the same material in similar conditions, if available. In this case, it is even more important to model the scatter associated to the fatigue life and to consider high-reliability curves. Another solution is to estimate the material parameters involved in the model through an optimization process aiming at minimizing the difference between the experimental N_f and the estimated N_f . In this case, however, the number of the experimental data should be as high as possible, depending on the number of parameters to be estimated. This could represent a future trend for the research on the models based on this approach. It is worth noting that other models based on the integration of the Paris law have been proposed in the literature,^{5,86,87} but they are more focused on the assessment of the number of cycles consumed in each stage of crack propagation rather than on assessing the stress–life relation and the P-S-N curves.

The analysis of all the available models has highlighted the relevance of assessing the crack origin and the failure mode to properly estimate the stress–life relation. The dependency between the defect size and the fatigue life must be also taken into account, since the defects control the VHCF response and are responsible for the large scatter associated with the VHCF failure data. Models for the LCF–VHCF life range should consider the possibility of two failure modes, with two different trends in the two regions. Almost all the models for duplex P-S-N curves consider two failure modes, that is, surface failure for LCF–HCF life range and internal failure from defect in the VHCF life range. On the other hand, in Li et al.⁶¹ and Lu et al.,⁸² three failure modes are considered. Indeed, for the internal failures, the authors differentiate between failures from defects without FGA formation and failures from defects with FGA formation, since they follow two different trends in an S–N plot. For this reason, fracture surfaces should be carefully investigated to verify the FGA formation, since, according to Li et al.⁶¹

and Lu et al.,⁸² the data would follow different distributions and different trends in an S–N plot.

It must be noted that some of the analyzed models^{37,45,61} in Section 3 show a horizontal asymptote at the end of a monotonic decreasing trend, that is, a fatigue limit. For example, in the model in Li et al.,⁶¹ three asymptotes are present, each corresponding to the “fatigue limit” for a specific failure mode. Similarly, the so-called “transition stress” can be considered as the fatigue limit for “surface failures.” However, differently from the fatigue limit models analyzed in Section 2, the horizontal asymptote present in the models described in this section is obtained through the fitting of the experimental data, that is, the experimental data show an asymptotic trend or an asymptotic trend is a priori supposed. This is the main difference between the fatigue limit assessed by considering the models for the stress–life in Section 3 (being the fatigue limit a fatigue strength) and the “fatigue limit” models analyzed in Section 2 and estimated through considerations on the crack initiation mechanisms close to the initial defect.

The models analyzed in this section can be considered valid for all VHCF failures, unless specified by the authors. However, the proposed models have been validated, generally, on a specific material or on materials with similar properties (e.g., high-strength steels and bearing steels spring steels). In order to prove the adaptability of the available models to different types of materials, the validation should be extended to a larger number of experimental datasets. Nonetheless, the majority of the investigated models has a general formulation that can be adapted to materials different from steels and showing similar failure modes. The models based on a statistical approach, for example, can be employed to fit datasets obtained by testing different materials: For example, the models in Paolino et al.,³⁶ validated on a H13 tool steel, have been adapted for modeling the stress–life relationship of AlSi10Mg specimens produced through additive manufacturing processes.⁵⁵ In general, a model can be applied to materials different from those considered for the validation. A careful validation, however, is strongly recommended. Otherwise, the use of the investigated models should be restricted to the test type and to the material considered for the validation.

Regarding the test type, the range of application of each model must be restricted depending on factors like the loading type, the testing method, and the stress ratio. For example, the influence of the mean stress has been investigated only in Ref.^{25,27,50,71,72} and all the investigated models consider only the case of a stress ratio equal to -1 . Literature models mainly deal with the fatigue response of specimens subjected to ultrasonic tension–compression

tests or to rotating bending tests.⁶ The influence of rotating bending or tension–compression loads is not so marked, being related mainly to the risk volume of the tested specimens, with specimens for rotating bending tests that are characterized by smaller risk volumes.^{30,38} Therefore, the models analyzed in this section can be generally employed for the estimation of the P–S–N curves of specimens subjected to ultrasonic tension–compression fatigue tests or to rotating bending tests, provided that the influence of the risk volume is considered. If this effect is not taken into account, the estimated P–S–N curves are valid only for the risk volume of the tested specimens.

Moreover, only in Akiniwa et al.⁴⁶ a model for the fatigue life of specimens subjected to torsion loads has been proposed.

Regarding the specimen condition, like the surface finishing, it has been never taken into account in the analyzed models. Indeed, specimens in the VHCF life range generally fail from internal inclusions or defects, with the surface roughness controlled through polishing or other processes, in order to enhance the crack initiation from internal defects. Therefore, the influence of surface finishing or roughness in VHCF can be hardly modeled, and accordingly, it has not been taken into account in the investigated models. The influence of other factors, like residual stresses, has not been modeled in all the analyzed papers.

In general, it can be concluded that most of the models available in the literature can be employed for steel materials subjected to a fully reversed tension–compression. More efforts should be made to extend the range of application of these models, by taking into account factors that strongly affect the VHCF response of parts in-service conditions.

To conclude, none of the papers analyzed in this review provide indications or a detailed methodology for the assessment of the design curve⁸⁸ in the VHCF life range. According to the industrial practice, the design curve is the lower confidence bound (e.g., 10%) for the P–S–N curve with high reliability (e.g., 10% quantile P–S–N curve) that, therefore, ensures an appropriate safety factor when components are designed against fatigue failures. More efforts should be made to provide methodologies for the definition of the “design curves” including the VHCF region, since they are used for the design of components and are therefore of fundamental importance in practical applications.

4 | CONCLUSIONS

In this paper, the models for the fatigue life in the VHCF region have been reviewed. In particular, the models

providing stress–life relation and, accordingly, that can be used for the assessment of the P–S–N curves have been analyzed in detail, for their relevance in the design against VHCF failures. The following conclusions can be drawn:

1. All the models for the fatigue limit show that the fatigue limit is inversely proportional to the defect size or to the FGA size. Indeed, in order to avoid the crack propagation from a defect in the VHCF region, the presence of the FGA must be taken into account and assessed experimentally or analytically. All the models show a similar expression, with different constant coefficients. The statistical scatter and the quantiles associated with the fatigue limit are not considered in the proposed formulations, apart from one model.
2. The models for the fatigue life can be classified depending on the approach followed to assess the stress–life relation. Four main approaches have been followed: an approach based on the fitting of the experimental data through a power-law relation, an approach based on the statistical assumption of the distribution of the fatigue life, a fracture mechanics approach, and an approach based on the integration of the Paris law.
3. The first approach, i.e., fitting of the experimental data with a power-law relation, is the easiest approach, with generally a limited number of parameters to be estimated. The experimental validations have confirmed that a power law is effective in modeling the fatigue life and that, if properly adapted, it can be exploited also to model the influence of defect size and of the stress ratio. A procedure for the quantile curves is generally not provided in the investigated models following this approach.
4. The second approach, a probabilistic approach involving the assumption of the statistical distribution of the fatigue life, has proved to be effective in assessing the P–S–N curves in the presence of multiple failure modes in the LCF–VHCF life range. The fatigue life is assumed to follow a log-normal or a Weibull distribution, both being effective in modeling the VHCF life. These models are more flexible than those belonging to other groups and can adapt better to the fatigue data, since not based on assumed materials parameters. Appropriate methodologies and strategies for parameter estimation are required.
5. Within the third group, all the models based on a fracture mechanics approach are included. The relation between the fatigue life, the applied stress, and the defect size is assessed by considering the stress intensity factor associated to the initial defect or the SIF threshold. These approaches have proved to be

effective; however, the material parameters in the SIF equation must be reliably known and should be estimated with specific experimental tests. The procedure for the estimation of the quantile of the P-S-N curves is generally not provided.

6. Within the fourth group, the models based on the integration of the Paris law are included. The stress-life relation is obtained through the integration of the Paris law in the three stages necessary for the crack formation and propagation up to failure. The fatigue life is generally approximated with the life consumed in the FGA formation, according to the experimental evidence. This approach has proved to be effective since it models the mechanism of crack initiation and propagation from defects, and accordingly, it takes into account the influence of defects on the fatigue life. However, the material parameters in the Paris law equation must be reliably known, even if this could be difficult, especially if the crack propagation within the FGA is modeled. Even for this group, the scatter associated to the experimental data is generally not modeled.

To conclude, all the available models have proved to be effective in assessing the fatigue limit or the stress-life relation. However, further validations are required to extend the models analyzed in the present paper for all the materials tested in VHCF life range. For example, the models developed for the fatigue life of parts that fail from defects in VHCF are to be considered valid for all the material showing this failure mechanism in VHCF. However, these models are validated on one experimental dataset, generally obtained by testing high-strength steels. For this reason, it seems that all the models have been developed to assess the P-S-N curves for steels or high-strength steels. The validity of these models for other materials has to be assumed, since it is not experimentally confirmed. This is a shortcoming of almost all the models developed in the literature that has to be faced in future research. Moreover, the influence of important factors, like the stress ratio, is considered only by a limited number of papers, despite its influence on the VHCF fatigue response. Another shortcoming evidenced from the analysis carried out in the paper is the complexity of the majority of the models, involving the estimation of a large number of coefficients to well fit the experimental data. This complexity could discourage their adoption in practical applications, with components subjected to VHCF loads that are still designed, for example, by employing high safety factors to lower the fatigue strength computed through traditional fatigue tests in the HCF life region. The simplification of the procedure for parameter estimation or the implementation of the

developed methodologies in automated tools would surely extend the application of the models for the P-S-N curves in VHCF even for the design of components, which is one of the primary objectives of the research. On the other hand, in general, no indications are provided for the assessment of the “design curves,” i.e., the lower confidence bound (e.g., 10%) for the P-S-N curve with high reliability (e.g., 10% quantile P-S-N curve), according to the industrial practice. More efforts should be made to define methodologies for the estimation of the “design curves” including the VHCF region, since they are used for the design of components and are therefore of fundamental importance in practical applications. This would surely help designers, opening the way towards a future standardization of the design methodologies against VHCF failures.

ACKNOWLEDGMENT

The research leading to these results has received funding from the European Union's Horizon 2020 innovation action program under Grant 101006844—Fatigue4Light project.

Open Access Funding provided by Politecnico di Torino within the CRUI-CARE Agreement.

AUTHOR CONTRIBUTIONS

Andrea Tridello analyzed the literature data and wrote the paper. Carlo Boursier Niutta helped to analyze the literature data, made addition to the paper, and revised the paper. Massimo Rossetto revised the paper and made addition to the paper. Filippo Berto revised the paper and made addition to the paper. Davide S. Paolino revised the paper, made addition to the paper, and supervised the work.

DATA AVAILABILITY STATEMENT


Data sharing is not applicable—no new data generated.

NOMENCLATURE

$a_{d,0}$	area of the initial defect size
a_{FGA}	size of the FGA surrounding the initial defect
cdf	cumulative distribution function
$f_{\sqrt{A_{d,0}}}$	pdf of the LEVD
F, F_Y	cdf of the fatigue life
$F_i(x)$	cdfs of the fatigue life associated to the i th failure mode
$F(x), F_1(x), F_2(x)$	cdfs of the fatigue life
$F_{X_i \sqrt{a_{d,0}}}(x_i; \sqrt{a_{d,0}})$	cdf of the fatigue limit
F_{X_i}	cdf of the transition stress

$F_{Y \sqrt{a_{d,0}}}(y; \mathbf{x}, \sqrt{a_{d,0}})$	cdf of the conditional fatigue life	x_l	logarithm of the fatigue limit
$F_{Y int}(y; \mathbf{x})$	cdf of the marginal distribution of the fatigue life	y	logarithm of the number of cycles to failure
$F_{Y surf}, F_{Y int}$	cdfs associated to the surface and internal failure modes	$\alpha, \alpha_H, \alpha_R, \alpha_{th,t}, a_j, a_{III}, \alpha_1, \alpha_2, b, b_j, b_{III}, \beta, c_{III}, B, C, \beta, c_H, c_j, c_{sl}, c_{th}, c_I, C_R, c, \delta, \hat{\gamma}, l, m, m_I, m, c_Y, m_Y, n_Y, s_{0,R}, \sigma_{f,j}, \sigma_{0,j}, \sigma_{f,III}, \sigma_Y, \sigma'_f$	material parameters
GBF	granular-bright facet	α_{th}	specific quantile
GP	generalized parameter (i.e., the uniaxial applied stress)	$\Delta\sigma_{th}$	threshold stress range
HCF	high-cycle fatigue	ε_a	strain amplitude
HV	Vickers hardness	$\varepsilon_a \cdot \left(\frac{2}{1-R}\right)^{1-\hat{\gamma}}$	Walker strain amplitude
<i>int, surf</i> (subscript)	internal and surface failure modes	$\mu_{X_l}, \sigma_{X_l}, \sigma_Y, \mu_{Y int}(x, \sqrt{a_{d,0}}), \mu_{X_l}(\sqrt{a_{d,0}}), \sigma_{X_l}$	parameters of the statistical distributions
k_d	SIF associated to the initial defect	Φ	cdf of a standardized normal distribution
K_{GBFth}	SIF threshold at the periphery of the GBF		
k_H	additional SIF modeling the influence of the hydrogen		
K_{th}	SIF threshold		
$k_{th,r}$	reduction SIF		
LCF	low-cycle fatigue		
LEVD	largest extreme value distribution		
n_{th}	number of failure modes		
N_f	number of cycles to failure		
N_L	fatigue life		
N_T	transition point		
ODA	optically dark area		
pdf	probability density function		
p_1, p_2	occurrence probability		
P-S-N curve	probabilistic S-N curve		
rv	random variable		
R	stress ratio		
R_i^{max}	radius of the largest inclusion within the material		
S_a	stress amplitude		
$S_{eq,CA}$ and $S_{eq,VA}$	equivalent stress for constant amplitude (CA) and variable amplitude (VA) tests		
s^{int}	internal fatigue limit		
s_l	fatigue limit		
SIF	stress intensity factor		
VHCF	very high cycle fatigue		
V_{90}	risk volume (volume subjected to a stress amplitude larger than the 90% of the largest applied stress)		

ORCID

Andrea Tridello  <https://orcid.org/0000-0003-3007-3377>
 Carlo Boursier Niutta  <https://orcid.org/0000-0002-7894-4752>

Massimo Rossetto  <https://orcid.org/0000-0003-3066-9680>

Filippo Berto  <https://orcid.org/0000-0001-9676-9970>

Davide S. Paolino  <https://orcid.org/0000-0002-4231-4580>

REFERENCES

1. Bathias C, Paris PC. *Gigacycle Fatigue in Mechanical Practice*. CRC Dekker; 2005.
2. Shanyavskiy A. Very-high-cycle-fatigue of in-service air-engine blades, compressor and turbine. *Sci China Press*. 2014;57(1): 19-29.
3. Mughrabi H. On “multi-stage” fatigue life diagrams and the relevant life-controlling mechanisms in ultrahigh-cycle fatigue. *Fatigue Fract Eng Mater Struct*. 2002;25(8-9):755-764.
4. Mughrabi H. Specific features and mechanisms of fatigue in the ultrahigh-cycle regime. *Int J Fatigue*. 2006;28(11): 1501-1508.
5. Akiniwa Y, Miyamoto N, Tsuru H, Tanaka K. Notch effect on fatigue strength reduction of bearing steel in the very high cycle regime. *Int J Fatigue*. 2006;28(11):1555-1565.
6. Sakai T, Lian B, Takeda M, et al. Statistical duplex S-N characteristics of high carbon chromium bearing steel in rotating bending in very high cycle regime. *Int J Fatigue*. 2010;32(3): 497-504.
7. Stanzl-Tschegg S. Very high cycle fatigue measuring techniques. *Int J Fatigue*. 2014;60:2-17.
8. Schmiedel A, Henkel S, Kirste T, Morgenstern R, Weidner A, Biermann H. Ultrasonic fatigue testing of cast steel G42CrMo4 at elevated temperatures. *Fatigue Fract Eng Mater Struct*. 2020;43(10):2455-2475.
9. Tridello A, Paolino DS, Chiandussi G, Goglio L. An innovative testing technique for assessing the VHCF response of

- adhesively bonded joints. *Fatigue Fract Eng Mater Struct.* 2019;42(1):84-96.
10. Tridello A, Ciardiello R, Paolino DS, Goglio L. Fatigue response up to 10^9 cycles of a structural epoxy adhesive. *Fatigue Fract Eng Mater Struct.* 2020;43(7):1555-1566.
 11. Cremer M, Zimmermann M, Christ HJ. High-frequency cyclic testing of welded aluminium alloy joints in the region of very high cycle fatigue (VHCF). *Int J Fatigue.* 2013;57:120-130.
 12. Zhu M-L, Liu L-L, Xuan F-Z. Effect of frequency on very high cycle fatigue behavior of a low strength Cr-Ni-Mo-V steel welded joint. *Int J Fatigue.* 2015;77:166-173.
 13. Backe D, Balle F, Eifler D. Fatigue testing of CFRP in the very high cycle fatigue (VHCF) regime at ultrasonic frequencies. *Compos Sci Tech.* 2015;106:93-99.
 14. Mayer H. Ultrasonic torsion and tension-compression fatigue testing: measuring principles and investigations on 2024-T351 aluminium alloy. *Int J Fatigue.* 2006;29(11):9-11.
 15. Marines-Garcia I, Doucet JP, Bathias C. Development of a new device to perform torsional ultrasonic fatigue testing. *Int J Fatigue.* 2007;28:1446-1455.
 16. Nikitin A, Bathias C, Palin-Luc T. A new piezoelectric fatigue testing machine in pure torsion for ultrasonic gigacycle fatigue tests: application to forged and extruded titanium alloys. *Fatigue Fract Eng Mater Struct.* 38(11):1294-1394.
 17. Vieira M, Freitas M, Reis L, Ribeiro AMR. Development of a very high cycle fatigue (VHCF) multiaxial testing device. *Procedia Struct Integrity.* 2016;37:131-137.
 18. Brugger C, Palin-Luc T, Osmond P, Blanc M. Ultrasonic fatigue testing device under biaxial bending. *Procedia Struct Integrity.* 2016;37:46-51.
 19. Li W, Sun R, Gao N, Wang P, Sakai T. Interior induced fatigue of surface-strengthened steel under constant and variable loading: failure mechanism and damage modeling. *Fatigue Fract Eng Mater Struct.* 2019;42(10):2383-2396.
 20. Murakami Y, Nomoto T, Ueda T. Factors influencing the mechanism of superlong fatigue failure in steels. *Fatigue Fract Eng Mater Struct.* 1999;22(7):581-590.
 21. Sakai T, Harada H, Oguma N. Crack initiation mechanism of bearing steel in very high cycle fatigue. In Proceedings of the ECF, Alexandroupolis, Greece, 3-7 July 2006; p. 16.
 22. Sakai T, Sato Y, Oguma N. Characteristic $S-N$ properties of high-carbon-chromium-bearing steel under axial loading in long-life fatigue. *Fatigue Fract Eng Mater Struct.* 2002;25(8-9):765-773.
 23. Shiozawa K, Morii Y, Nishino S. Subsurface crack initiation and propagation mechanism under the super-long fatigue regime for high speed tool steel (JIS SKH51) by fracture surface topographic analysis. *JSME Int J.* 2006;49(1):1-10.
 24. Sippel JP, Kerscher E. Properties of the fine granular area and postulated models for its formation during very high cycle fatigue—a review. *Appl Sci.* 2020;10:1-27.
 25. Bandara CS, Siriwardane SC, Dissanayake UI, Dissanayake R. Fatigue failure predictions for steels in the very high cycle region—a review and recommendations. *Eng Fail Anal.* 2014;2014(45):421-435.
 26. Hong Y, Sun C. The nature and the mechanism of crack initiation and early growth for very-high-cycle fatigue of metallic materials—an overview. *Theor Appl Fract Mec.* 2017;92:331-350.
 27. Sun C, Lei Z, Xie J, Hong Y. Effects of inclusion size and stress ratio on fatigue strength for high-strength steels with fish-eye mode failure. *Int J Fatigue.* 2013;48:19-27.
 28. Liu YB, Yang ZG, Li YD, et al. Dependence of fatigue strength on inclusion size for high-strength steels in very high cycle fatigue regime. *Mater Sci Eng A.* 2009;517(1-2):180-184.
 29. Liu YB, Li YD, Li SX, et al. Prediction of the $S-N$ curves of high-strength steels in the very high cycle fatigue regime. *Int J Fatigue.* 2010;32(8):1351-1357.
 30. Murakami Y. *Metal Fatigue: Effects of Small Defects and Non-metallic Inclusions.* Elsevier Ltd; 2002.
 31. Spriestersbach D, Kerscher E. The role of local plasticity during very high cycle fatigue crack initiation in high-strength steels. *Int J Fatigue.* 2018;111:93-100.
 32. Murakami Y, Yamashita Y. Prediction of life and scatter of fatigue failure originated at nonmetallic inclusions. *Procedia Eng.* 2014;74:6-11.
 33. Chapetti MD, Tagawa T, Miyata T. Ultra-long cycle fatigue of high-strength carbon steels part I: review and analysis of the mechanism of failure. *Mater Sci Eng A.* 2003;356(1-2):227-235.
 34. Chapetti MD, Tagawa T, Miyata T. Ultra-long cycle fatigue of high-strength carbon steels part II: estimation of fatigue limit for failure from internal inclusions. *Mater Sci Eng A.* 2003;356(1-2):236-244.
 35. Liu YB, Yang ZG, Li YD, et al. On the formation of GBF of high-strength steels in the very high cycle fatigue regime. *Mater Sci Eng A.* 2008;497(1-2):408-415.
 36. Paolino DS, Tridello A, Chiandussi G, Rossetto M. $S-N$ curves in the very-high-cycle fatigue regime: statistical modeling based on the hydrogen embrittlement consideration. *Fatigue Fract Eng Mater Struct.* 2016;39(11):1319-1336.
 37. Paolino DS, Tridello A, Chiandussi G, Rossetto M. Estimation of P-S-N curves in very-high-cycle fatigue: statistical procedure based on a general crack growth rate model. *Fatigue Fract Eng Mater Struct.* 2018;41(4):718-726.
 38. Tridello A, Paolino DS, Chiandussi G, Rossetto M. Effect of electrosag remelting on the VHCF response of an AISI H13 steel. *Fatigue Fract Eng Mater Struct.* 2017;40(11):1783-1794.
 39. Paolino DS, Tridello A, Chiandussi G, Rossetto M. Crack growth from internal defects and related size-effect in VHCF. *Fatigue Fract Eng Mater Struct.* 2017;40:1783-1794.
 40. Paolino DS, Tridello A, Chiandussi G, Rossetto M. A general statistical model for the description of the hydrogen assisted crack initiation in the VHCF regime. Proceedings of the Seventh International Conference on Very High Cycle Fatigue (VHCF 7), Dresden (Germany), 3-5 July 2017.
 41. Nishijima S, Kanazawa K. Stepwise $S-N$ curve and fish-eye failure in gigacycle fatigue. *Fatigue Fract Eng Mater Struct.* 1999;22(7):601-607.
 42. Hanaki S, Yamashita M, Uchida H, Zako M. On stochastic evaluation of $S-N$ data based on fatigue strength distribution. *Int J Fatigue.* 2010;32(3):605-609.
 43. Ishihara S, Lu L, Shiozawa K. Ishihara $S-N$ curve characteristics and subsurface crack initiation behaviour in ultra-long life fatigue of a high carbon-chromium bearing steel. *Fatigue Fract Eng Mater Struct.* 2001;24(12):781-790.

44. Sonsino CM. Course of S-N-curves especially in the high-cycle fatigue regime with regard to component design and safety. *Int J Fatigue*. 2007;29(12):2246-2258.
45. Paolino DS, Chiandussi G, Rossetto M. A unified statistical model for S-N fatigue curves: probabilistic definition. *Fatigue Fract Eng Mater Struct*. 2013;36(3):187-201.
46. Akiniwa Y, Stanzl-Tschegg S, Mayer H, Wakita M, Tanaka K. Fatigue strength of spring steel under axial and torsional loading in the very high cycle regime. *Int J Fatigue*. 2008;30(12):2057-2063.
47. Tanaka K, Akiniwa Y. Fatigue crack propagation behaviour derived from S-N data in very high cycle regime. *Fatigue Fract Eng Mater Struct*. 2002;25(8-9):775-784.
48. Mayer H, Haydn W, Schuller R, Issler S, Furtner B, Bacher-Höchst M. Very high cycle fatigue properties of bainitic high carbon-chromium steel. *Int J Fatigue*. 2009;31(2):242-249.
49. Wang J, Yang Y, Yu J, Wang J, Du F, Zhang Y. Fatigue life evaluation considering fatigue reliability and fatigue crack for FV520B-I in VHCF regime based on fracture mechanics. *Metals (Basel)*. 2020;10(3):371.
50. Schönbauer BM, Fitzka M, Karr U, Mayer H. Variable amplitude very high cycle fatigue of 17-4PH steel with a stepwise S-N curve. *Int J Fatigue*. 2021;142:105963.
51. Schönbauer BM, Yanase K, Endo M. VHCF properties and fatigue limit prediction of precipitation hardened 17-4PH stainless steel. *Int J Fatigue*. 2016;88:205-216.
52. Chantier I, Bobet V, Billardon R, Hild F. A probabilistic approach to predict the very high-cycle fatigue behaviour of spheroidal graphite cast iron structures. *Fatigue Fract Eng Mater Struct*. 2000;23(2):173-180.
53. Qian G, Zhou C, Hong Y. A model to predict S-N curves for surface and subsurface crack initiations in different environmental media. *Int J Fatigue*. 2015;71:35-44.
54. Wu T, Yao W, Xu C. A distribution model of ultra-high cycle fatigue property based on crack density for braided CFRP. *Compos Struct*. 2021;256:113037.
55. Tridello A, Fiocchi J, Biffi CA, et al. VHCF response of Gaussian SLM AlSi10Mg specimens: effect of a stress relief heat treatment. *Int J Fatigue*. 2019;124:435-443.
56. Weixing Y, Shenjie G. VHCF test and life distribution of aluminum alloy LC4CS. *Int J Fatigue*. 2008;30(1):172-177.
57. Zhao YX, Yang B, Feng MF, Wang H. Probabilistic fatigue S-N curves including the super-long life regime of a railway axle steel. *Int J Fatigue*. 2009;31(10):1550-1558.
58. American Association of State Highway and Transportation Officials. *Standard Specifications for Highway Bridges*. American Association of State Highway and Transportation Officials; 1988.
59. European Convention for Constructional Steel Works. *ECCS-Technical Committee 6-Fatigue. Recommendation for the Fatigue Design of Steel Structures*. European Convention for Constructional Steel Works; 1985.
60. Bomas H, Burkart K, Zoch HW. Evaluation of S-N curves with more than one failure mode. *Int J Fatigue*. 2011;33(1):19-22.
61. Li W, Sun Z, Zhang Z, Deng H, Sakai T. Evaluation of crack growth behavior and probabilistic S-N characteristics of carburized Cr-Mn-Si steel with multiple failure modes. *Mater Des*. 2014;64:760-768.
62. Li W, Sakai T, Deng H. Statistical evaluation of very high cycle fatigue property of high carbon chromium bearing steel under axial loading. *Mater Sci Technol (United Kingdom)*. 2016;32:1094-1099.
63. Muniz-Calvente M, Fernández-Canteli A, Pyttel B, Castillo E. Probabilistic assessment of VHCF data as pertaining to concurrent populations using a Weibull regression model. *Fatigue Fract Eng Mater Struct*. 2017;40(11):1772-1782.
64. Fernández-Canteli A, Castillo E. A general regression model for lifetime evaluation and prediction. *Int J Fract*. 2001;107(2):117-137.
65. National Institute for Materials Science. NIMS Fatigue Data Sheet No. 98, Data sheet on giga-cycle fatigue properties of Ti-6Al-4V (1100 MPa class) titanium alloy, National Institute for Materials Science, Tokyo, 2005.
66. Paolino DS, Tridello A, Geng HS, Chiandussi G, Rossetto M. Duplex S-N fatigue curves: statistical distribution of the transition fatigue life. *Frat Integrita Strutt*. 2014;30(30):417-423.
67. Fernández-Canteli A, Blasón S, Pyttel B, Muniz-Calvente M, Castillo E. Considerations about the existence or non-existence of the fatigue limit: implications on practical design. *Int J Fract*. 2020;223(1-2):189-196.
68. Paolino DS, Tridello A, Chiandussi G, Rossetto M. Statistical estimation of duplex S-N curves. *Key Eng Mater*. 2016;664:285-294.
69. Sun C, Zhang X, Liu X, Hong Y. Effects of specimen size on fatigue life of metallic materials in high-cycle and very-high-cycle fatigue regimes. *Fatigue Fract Eng Mater Struct*. 2016;39(6):770-779.
70. Furuya Y. Notable size effects on very high cycle fatigue properties of high-strength steel. *Mater Sci Eng A*. 2011;528(15):5234-5240.
71. Apetre N, Arcari A, Dowling N, Iyyer N, Phan N. Probabilistic model of mean stress effects in strain-life fatigue. *Procedia Eng*. 2015;114:538-545.
72. Arcari A, Apetre N, Dowling N, et al. Variable amplitude fatigue life in VHCF and probabilistic life predictions. *Procedia Eng*. 2015;114:574-582.
73. Dowling NE. Mean stress effects in strain life fatigue. *Fatigue Fract Engng Mater Struct*. 2009;32(12):1004-1019.
74. Pinto H, de Jesus AMP, Fernandez-Canteli A, Castillo E, Pereira HFSG. Analysis of constant and variable amplitude strain-life data using a novel probabilistic Weibull regression model. *J Pressure Vessel Technol*. 2010;132(6):061401.
75. Castillo E, Fernandez-Canteli A. A general regression model for lifetime evaluation and prediction. *Int J Fract*. 2001;107(2):117-137.
76. Castillo E, Fernandez-Canteli A. *A Unified Statistical Methodology for Modeling Fatigue Damage*. Springer; 2009.
77. Liu X, Sun C, Hong Y. Effects of stress ratio on high-cycle and very-high-cycle fatigue behavior of a Ti-6Al-4V alloy. *Mater Sci Eng A*. 2015;622:228-235.
78. Chen D, Nisitani H, Mori K. Three-dimensional surface and interior cracks. In: Murakami Y, ed. *Stress Intensity Factor Handbook*. Vol. 3. Society of Materials Science; 1993:661-662.
79. Wang QY, Bathias C, Kawagoishi N, Chen Q. Effect of inclusion on subsurface crack initiation and gigacycle fatigue strength. *Int J Fatigue*. 2002;24(12):1269-1274.

80. Wang QY, Berard JY, Dubarre A, Baudry G, Rathery S, Bathias C. Gigacycle fatigue of ferrous alloys. *Fatigue Fract Eng Mater Struct*. 1999;22(8):667-672.
81. Kolyshkin A, Grigorescu A, Kaufmann E, Zimmermann M, Christ HJ. Development of a probabilistic model for the prediction of fatigue life in the very high cycle fatigue (VHCF) range based on inclusion population. *Procedia Struct Integr*. 2016;2: 1085-1092.
82. Lu LT, Zhang JW, Shiozawa K. Influence of inclusion size on S-N curve characteristics of high-strength steels in the gigacycle fatigue regime. *Fatigue Fract Eng Mater Struct*. 2009; 32(8):647-655.
83. Schuller R, Fitzka M, Irrasch D, Tran D, Pennings B, Mayer H. VHCF properties of nitrided 18Ni maraging steel thin sheets with different Co and Ti content. *Fatigue Fract Eng Mater Struct*. 2015;38(5):518-527.
84. Sun C, Liu X, Hong Y. A two-parameter model to predict fatigue life of high-strength steels in a very high cycle fatigue regime. *Acta Mech Sin*. 2015;31(3):383-391.
85. Tridello A, Paolino DS. A new statistical software for the estimation of P-S-N curves in presence of defects: statistical models and experimental validation. *IOP Conf Ser Mater Sci Eng*. 2021; 1038:012029.
86. Marines-Garcia I, Paris PC, Tada H, Bathias C, Lados D. Fatigue crack growth from small to large cracks on very high cycle fatigue with fish-eye failures. *Eng Fract Mech*. 2008;75(6): 1657-1665.
87. Pineau A, Antolovich SD. Probabilistic approaches to fatigue with special emphasis on initiation from inclusions. *Int J Fatigue*. 2016;93:422-434.
88. Shen CL, Wirshing PH, Cashman GT. Design curve to characterize fatigue strength. *J Eng Mater Technol*. 1996;1996(118): 535-541.

How to cite this article: Tridello A, Boursier Niutta C, Rossetto M, Berto F, Paolino DS. Statistical models for estimating the fatigue life, the stress-life relation, and the P-S-N curves of metallic materials in Very High Cycle Fatigue: A review. *Fatigue Fract Eng Mater Struct*. 2022;45(2): 332-370. doi:10.1111/ffe.13610